Downregulation of the TGF-β pseudoreceptor BAMBI in non-small cell lung cancer enhances TGF-β signaling and invasion

Sebastian Marwitz[(1,6)*], Sofia Depner[(2,3,7)*], Dmytro Dvornikov[(2,7)*], Ruth Merkle[(2,3,7)], Magdalena Szczygieł [(2,7)], Karin Müller-Decker[(10)], Philippe Lucarelli[(2,7)†], Marvin Wäsch[(2,7)], Heimo Mairbäurl[7,8], Klaus F. Rabe[(4,6,9)], Christian Kugler[(4,6)], Ekkehard Vollmer[(1,6)], Martin Reck[(4,6)], Swetlana Scheufele[(5,6)], Maren Kröger[(5,6)], Ole Ammerpohl[(5,6)], Reiner Siebert[(5,6)], Torsten Goldmann[(1,6)$], Ursula Klingmüller[(2,3,7)$]

1: Pathology of the University Hospital of Luebeck and the Leibniz Research Center Borstel, 23538 Luebeck and 23845 Borstel, Germany

2: Systems Biology of Signal Transduction, German Cancer Research Center, Im Neuenheimer Feld 280, 69120 Heidelberg, Germany

3: BIOQUANT, University of Heidelberg, Im Neuenheimer Feld 267, 69120 Heidelberg, Germany

4: LungenClinic Grosshansdorf, Wöhrendamm 80, 22927 Groβhansdorf, Germany

5: Institute of Human Genetics, Christian-Albrechts-University Kiel and University Hospital Schleswig-Holstein, Campus Kiel, Schwanenweg 24, 24105 Kiel, Germany

6: Airway Research Center North (ARCN), Member of the German Center for Lung Research (DZL), Germany

7: Translational Lung Research Center Heidelberg (TLRC), German Center for Lung Research (DZL), Heidelberg, Germany

8: Medical Clinic VII, Sports Medicine, University Hospital Heidelberg, Im Neuenheimer Feld 410, 69120 Heidelberg, Germany

9: Christian Albrechts University Kiel, Christian-Albrechts-Platz 4, 24118 Kiel, Germany

10: Tumor Models, German Cancer Research Center, Im Neuenheimer Feld 280, 69120 Heidelberg, Germany

Present address:
†: Systems Biology Group, Life Sciences Research Unit, University of Luxembourg, Belvaux, Luxembourg
*: These authors contributed equally to this work.
$: These authors share senior authorship.

Corresponding author:
Ursula Klingmüller
Mailing address: Im Neuenheimer Feld 280, 69120 Heidelberg
Email: u.klingmueller@dkfz-heidelberg.de
Phone: +49-6221-424481
Fax: +49-6221-424488

Running headline: Role of BAMBI in lung cancer

Disclosure of Potential Conflicts of Interests
No potential conflicts of interest were disclosed by any of the authors.

ABSTRACT

Non-small cell lung cancer (NSCLC) is characterized by early metastasis and has the highest mortality rate among all solid tumors, with the majority of patients diagnosed at an advanced stage where curative therapeutic options are lacking. In this study, we identify a targetable mechanism involving TGF-β elevation that orchestrates tumor progression in this disease. Substantial activation of this pathway was detected in human lung cancer tissues with concomitant downregulation of BAMBI, a negative regulator of the TGF-β signaling pathway. Alterations of epithelial-to-mesenchymal transition (EMT) marker expression were observed in lung cancer samples compared to tumor-free tissues. Distinct alterations in the DNA methylation of the gene regions encoding TGF-β pathway components were detected in NSCLC samples compared to tumor-free lung tissues. In particular, epigenetic silencing of BAMBI was identified as a hallmark of NSCLC. Reconstitution of BAMBI expression in NSCLC cells resulted in a marked reduction of TGF-β-induced EMT, migration and invasion *in vitro*, along with reduced tumor burden and tumor growth *in vivo*. In conclusion, our results demonstrate how BAMBI downregulation drives the invasiveness of NSCLC, highlighting TGF-β signaling as a candidate therapeutic target in this setting.

INTRODUCTION

Primary lung cancer is one of the most common malignancies worldwide and has the highest mortality rate among all solid tumors (1) with non-small cell lung cancer (NSCLC) as the most frequent tumor type comprising approximately 80% of diagnosed cases. Due to the lack of characteristic early symptoms, 60% of lung carcinomas are detected in a progressed or already metastasized state (2) with a 5-year-survival of only 16% independent of the tumor stage and size (3). Therapeutic interventions depend on the tumor stage and only at early stages of tumor progression patients are eligible for curative surgery. The majority of patients are treated with chemotherapy. Still, the available therapies for lung cancer are very limited, and rapid progression due to resistance to therapy is a major clinical challenge. To develop novel therapeutic approaches, a detailed understanding of the mechanisms contributing to lung cancer progression is essential.

The process of epithelial-to-mesenchymal transition (EMT) is known to contribute to several lung diseases, such as idiopathic pulmonary fibrosis, asthma and chronic obstructive pulmonary disease (COPD) (4). With respect to cancer progression, EMT has been observed in cancers of the breast or prostate (5), but this process has not yet been comprehensively studied in the context of lung cancer tissues.

TGF-β is a cytokine with pleiotropic effects during development, inflammation, as well as tissue homeostasis. Additionally, it exerts tight tempo-spatial control of differentiation, apoptosis and proliferation in both, epithelial and immune cells (6). Furthermore, TGF-β is known to play a central role in the induction of the EMT. Under pathological conditions such as lung cancer, TGF-β plays a dual role in the course of carcinogenesis. At primary stages it acts as a tumor suppressor inducing apoptosis and controlling proliferation, while at later stages the tumor promoting effects take over and promote EMT, invasion and metastasis. Furthermore, TGF-β has immunosuppressive properties and may enable cancer cells to evade the immune responses (7). The canonical TGF-β cascade signals through both TGF-β receptors type 1 (TGFBR1) and type 2 (TGFBR2). Upon binding of the ligand to TGFBR2, TGFBR1 is phosphorylated and recruits the receptor (R)-SMADS SMAD2 and SMAD3, which form a complex with the common SMAD, SMAD4, migrate to the nucleus and stimulate target gene expression. Negative regulation is exerted by the inhibitory SMADs, such as SMAD7 (8), or at the receptor level by the pseudo-receptor bone morphogenetic protein and activin membrane-bound inhibitor (BAMBI), which is homologous to TGFBR1 but lacks an active kinase domain (9).

In the context of lung disease, the over-expression of BAMBI has been observed in the tissues of COPD patients and hypothesized to control local inflammation and remodeling processes (10). The expression of BAMBI at high levels has also been detected in colorectal cancer (11) and ovarian cancer (12) and has been linked to metastasis in colorectal cancer (13). By contrast, BAMBI is epigenetically silenced in high grade bladder cancer (14) and absent from breast cancer (15). Hence, the specific contribution of BAMBI to tumor progression remains unresolved.

In this study, we comprehensively examined the TGF-β signaling pathway in lung cancer and, using the negative regulator BAMBI as an example, demonstrated that altered TGF-β signaling contributes to malignant processes such as EMT, migration and invasion. The results suggest that TGF-β signaling is a promising therapeutic target in lung cancer.

MATERIALS AND METHODS

Patient material, ethical issue and tissue processing

Lung tissue samples were obtained from patients who underwent lobectomy or pneumectomy due to therapeutic interventions at the LungenClinic Grosshansdorf, Germany. Residual tumor and tumor-free lung tissues not needed for diagnostic purposes were HOPE-fixed and paraffin-embedded according to manufacturer´s instructions (DCS Innovative Systeme, Hamburg, Germany). The use of patient materials was approved by local ethics committee of the University of Lübeck (AZ 12-220), Germany. For analysis in cancer tissues, 133 archived lung cancer specimens of either adenocarcinoma or squamous cell carcinoma diagnosis were randomly selected and subjected to immunohistochemistry. The gender ratio was 43 female vs. 90 male patients and the mean age at time of diagnosis was 66.06 years (± 9.9). Among the investigated lung cancer specimen, 74 were squamous cell carcinomas (55.6%) and 59 adenocarcinomas (44.4%). As controls, 23 cases of tumor-free lung specimen were included, four of which were paired with lung cancer specimen (Supplementary Table 2). A detailed overview of the patient characteristics as well TNM staging and other relevant information can be found in Supplementary Table 6.

Isolation of primary alveolar epithelial cells type II (AECII)

Tumor-free lung tissues from surgical specimens of patients who underwent pneumectomy or lobectomy at the LungenClinic Grosshansdorf were used for isolation of primary AECII. Fresh tissues were rinsed with sterile PBS to remove excess blood and stored in RPMI 1640 (Life Technologies) cell culture medium, supplemented with 10% FCS and 1% penicillin/streptomycin at 4°C until further use. To extract AECII, the tissue was manually dissected with surgical razors and rinsed with AECII buffer (1.9 mM calcium chloride dihydrate; 1.3 mM magnesium sulfate heptahydrate; 136 mM sodium chloride; 6.1 mM kalium chloride; 3.2 mM di sodium hydrogen phosphate; 6.1 mM glucose and 9.9 mM HEPES) over a sieve to remove residual blood. Tissue pieces were dissociated by incubation for 60 min at 37°C and 5% CO_2 in AECII buffer supplemented with 2 mg/ml Dispase II (Roche Applied Sciences, Mannheim, Germany) under constant stirring. The lung tissue pieces were further filtered through nylon gaze of decreasing pore size (100 µm, 50 µm, 20 µm) and finally sedimented for 15 min at 478 *g* at room temperature. The resulting cell pellet was resuspended in 50 ml of AECII buffer supplemented with 0.001% Accutase (MilliPore, Darmstadt, Germany) (v/v) and 20 µg/ml DNAse I (Roche Applied Sciences, Mannheim, Germany). Each 10 ml of this suspension was applied onto 10 ml Biocoll gradient solution (Biochrome,) and centrifuged for 25 min at 478 *g* and room temperature. The resulting interphase was washed with AECII buffer at 478 *g* for 15 min at 4°C and finally resuspended in cell culture medium. Each 5×10^7 cells were seeded on 6-cm petri dishes and incubated for 20 min. at 37°C in an incubator to allow adherence of immune cells. 1×10^7 of non-adhered cells were resuspended in 80 µl MACS-buffer (PBS pH 7.2 with 0.5% BSA and 2 mM EDTA), mixed with 20 µl anti-CD45 conjugated para-magnetic beads (Miltenyi, Bergisch Gladbach, Germany) and finally incubated on a rotating device for 15 min. Depletion of CD45 positive immune cells with LD columns (Miltenyi, Bergisch Gladbach, Germany) was conducted according to manufacturer´s instructions.

Production of tissue microarray and cellblocks

Tissue microarrays from HOPE-fixed, paraffin-embedded tissues were produced as described by Goldmann *et al.* (46). HOPE-fixed cells were dehydrated and subsequently paraffin-embedded according to Marwitz *et al.* (47) to produce cell blocks for immunocytochemistry.

Immunohistochemistry

HOPE-fixed, paraffin-embedded tissues and tissue microarrays were cut on a microtome (Leica SM 2000) to obtain sections of 1 µm thickness and mounted on SuperFrost+ (Menzel Gläser) glass slides. Subsequent deparaffinization was done by incubation in 100% isopropanol for 10 min at 65°C. Sections were shortly air dried, rehydrated in 70% acetone for 10 min at 4°C and transferred into distilled water for 10 min at 4°C. Endogenous peroxidases were blocked by incubation in 3% H_2O_2 for 10 min. Primary antibodies were diluted with antibody diluent (Zytomed Systems) as following: mouse anti-BAMBI monoclonal (clone 4e8, eBioscience) 1:100; rabbit anti-BAMBI polyclonal (Sigma-Aldrich) 1:100; rabbit anti-SMAD2 (clone D43B4, Cell Signaling Technologies), anti-phospho-SMAD2 (clone 138D4, Cell Signaling Technologies), rabbit anti-SMAD3 (clone C67H9, Cell Signaling Technologies), rabbit anti-phospho-SMAD3 (C25A9, Cell Signaling Technologies), rabbit anti-SMAD4 (clone EP618Y, Cell Signaling Technologies), rabbit anti-TGF-β polyclonal (Abcam), mouse anti-SNON monoclonal (clone 2F6, Abcam), rabbit anti-E-cadherin monoclonal (clone 24E10, Cell Signaling Technologies), mouse anti-N-cadherin monoclonal (5D5, Abcam) and rabbit anti-HMGA1 monoclonal (clone EPR7839, Abcam) all 1:200; mouse anti-SMAD7 (clone 293039, R&D Systems) and rabbit anti-Osteopontin/SPP1 polyclonal (Zytomed Systems) all 1:100. For visualization, a HRP-conjugated polymer kit was used according to manufacturer`s instructions (ZytoChemPlus Kit, Zytomed Systems). Chromogenic reaction was conducted with permanent AEC (Permanent AEC Kit, Zytomed Sytems) and stopped with distilled water. The slides were subsequently dehydrated in graded series of ethanol (70%, 90%, 2× 95%, 2× 100%, xylene) and mounted with Pertex (Medite). Negative controls were included by omission of primary antibody in each staining and photomicrographs were taken with a CCD camera (Infinity 4, Lumenera). Contrast and brightness of images were adjusted using FixFoto software (Joachim Koopman Software). For evaluation of target expression, a semi-quantitative score was applied based on histology analysis of the whole specimen as following: negative (0), focal and weak expression (1), frequent intermediate expression (2), strong expression and dominating feature of specimen (3). The whole specimen was considered for evaluation of microscopic slides.

Immunofluorescence staining of paraffin-embedded tissues

Cutting, mounting and deparaffinization of tissue slides were conducted as described above. Rehydrated slides were incubated with either rabbit anti-pSMAD3 (clone C25A9, Cell Signaling Technologies) and mouse anti-N-cadherin (clone 5D5, Abcam) or rabbit anti-E-cadherin (clone 24E10, Cell Signaling Technologies) and mouse anti-N-cadherin (clone 5D5, Abcam) all diluted 1:200 in antibody diluent (Zytomed Systems) for 45 min at room temperature in a humid chamber. Detection of primary antibodies was done with goat anti-rabbit and goat anti-mouse secondary antibodies conjugated with Alexa488 (Life Technologies) or Tetramethylrhodamine (Life Technologies), respectively diluted 1:200 in antibody diluent for 45 min. Thoroughly washed slides were mounted with VectaShield mounting media with DAPI (Vectorlabs) and kept in the dark at 4°C until read-out.

RNA and DNA isolation

The samples for epigenetic studies were enriched for tumor cells by micro-dissection of H&E-stained lung cancer specimens under a microscope. Dissected cells were transferred into a 1.5-ml reaction tube and DNA isolation was done with the QIAmp Mini Kit (Qiagen) according to manufacturer`s instructions. For transcriptome analysis and qRT-PCR, sections from paraffin blocks were cut on a microtome and deparaffinized prior to RNA isolation. Briefly, each sample was rotated with 1 ml xylene for 10 min at RT. The tissue was pelleted by centrifugation at 12,000 *g* for 5 min, the supernatant discarded and the procedure repeated once. Deparaffinized tissue was washed twice with 1 ml 100% ethanol for 10 min at RT. Residual ethanol was removed by vacuum centrifugation and dried pellets were homogenized in RLT buffer with an electronic pestle (VWR). RNA was isolated using the RNeasy Mini Kit (Qiagen) according to manufacturer`s instructions. For qRT-PCR of the cell lines, RNA was extracted using the RNeasy Mini Plus Kit (Qiagen) according to the manufacturer's instructions.

Microarray analysis

RNA integrity for microarray analysis was determined using the Agilent Bioanalyzer with the RNA Nano 6000 Kit according to manufacturer`s instructions (Agilent). Transcriptome analysis was conducted as described in the One-Color Microarray-Based Gene Expression Analysis Low Input Quick Amp Labeling protocol version 6.6. Shortly, 200 ng of total RNA was mixed with the RNA Spike-In Mix as internal control (Agilent One Color RNA Spike-In Kit) and reverse transcribed into cDNA by MMLV reverse transcriptase. Labeling with Cy3-CTP was conducted with T7 RNA polymerase. Cy3 labeled cRNA was purified using RNeasy Mini Kit and specific activity was calculated using a NanoDrop 2000 spectrophotometer (Thermo Fisher Scientific). 1650 ng of labeled cRNA was hybridized on Agilent Human Gene Expression 4x44k V2 arrays and scanned with an Agilent SureScan microarray scanner. Raw data was extracted with Agilent Feature Extraction software v11 applying 1-color Green Gene Expression protocol. For hierarchical clustering and heat map analysis, Agilent GeneSpring GX software version 12.6 was used. Hierarchical clustering was computed with GeneSpring GX 12.6 on entities (genes) and conditions (samples) with squared Euclidean distance metrics and Ward`s linkage rule. Quantile-normalized gene expression data was computed using DirectArray software (Oaklabs). Microarray results are deposited to the GEO database (GEO accession number GSE74706).

cDNA Synthesis and quantitative Real-Time PCR (qRT-PCR)

cDNA was generated from 1 µg of total RNA using Maxima First Strand cDNA Synthesis Kit (Thermo Scientific) for tissues and High Capacity cDNA Reverse Transcription Kit (Applied Biosystems) for cell lines according to manufacturer`s instructions. cDNA templates were analyzed by qRT-PCR on a LightCycler 480 (Roche Applied Science) cycler (cell lines and tissues) using the LightCycler 480 Probes Master with final 0.4 µM primer and 0.2 µM FAM-labeled hydrolysis probes (Universal Probe Library, Roche Applied Science). Crossing point values were calculated using the second-derivative-maximum method of the LightCycler 480 Basic Software (Roche Applied Science). Concentrations were normalized using the geometric mean of β-glucuronidase (*GUSB*) and esterase D (*ESD*) or glyceraldehyde-3-phosphate dehydrogenase (*GAPDH*) and glucose-6-phosphate 1-dehydrogenase D (*G6PD*) for cell lines and the geometric mean of ESD, *GAPDH*, phosphoglycerate kinase 1 (*PGK1*), hypoxanthine-guanidine phosphoribosy ltransferase (*HPRT*) and TATAA-box-binding protein (*TBP*) for tissues. The *BAMBI* mRNA quantification for different cell types was performed in

independent experiments with at least one cell line overlapping to put the other cell types into perspective. Primers were designed using the UniversalProbe Library Assay Design Center (Roche Applied Science). The PCR primer sequences used are listed in Supplementary Table 7.

DNA methylation analysis

Methylation analysis of Hope-fixed, paraffin-embedded tissues was conducted as described elsewhere (48). Briefly, bisulfite conversion of genomic DNA applying the EZ DNA Methylation kit (ZymoResearch, Irvine, CA, USA) as well as subsequent DNA methylation analysis using the Infinium HumanMethylation450k BeadChip (Illumina Inc., San Diego, CA, USA) were performed according the manufacturers' instructions. The HumanMethylation450K BeadChip aims at assaying more than 480,000 CpG sites in parallel. DNA methylation data were analyzed using the GenomeStudio software (v2011.1; methylation modul 1.9.0; Illumina, Inc.) applying the default settings. The array's intrinsic controls were used for normalization of the data, no further background subtraction or normalization steps were performed. Identification of differentially methylated CpG loci, PCA as well as hierarchical cluster analysis were performed using the OMICS Explorer 2.3 (Version 2.3(45), Qlucore, Lund, Sweden) software using DNA methylation values (average beta values) obtained from the GenomeStudio software. HumanMethylation450k BeadChip results are deposited to the GEO database (GEO accession number GSE75008).

To validate the DNA methylation values detected by HumanMethylation450K BeadChip, DNA from 14 lung carcinoma samples as well as their corresponding normal controls were bisulfite converted using the EpiTect Kit (Qiagen, Hilden, Germany) following the manufacturer's instruction. Subsequently, bisulfite pyrosequencing of the selected loci was performed as described by (49) to determine the DNA methylation state at cg05046589 (forward primer: ttttttaggggtgaggttttaggtag; reverse primer (biotinylated): aaccactcaatcaaaatacatctttaca; sequencing primer: aggttttaggtaggtg), cg17482424 (forward primer: aggaaataggtattagtatgatggtagta; reverse primer (biotinylated): actttacaacctacccctttt; sequencing primer: gagttgatttttttttaaagagtt) and cg07232003 (forward primer: tgtaaagttagatttggaatgtatgg; reverse primer (biotinylated): actcaaaaaaccttcaaactattca; sequencing primer: tttattggggtatgtatag).

Selection of genes involved in the TGF-β signaling pathway and EMT

The *a priori*-generated lists of genes for microarray and methylation analyses for TGF-β pathway members were retrieved from public databases (Wikipathways and KEGG) as well as from literature search. Since the databases contained no available list for EMT genes, the set of genes was adapted from commercially available EMT array sets and literature search.

Comparison of DNA methylation and gene expression data

To analyze correlation between differential methylation and aberrant gene expression in TGF-β pathway member genes the mean differential methylation in all tumor-control sample pairs was determined for each locus. Only loci with mean differential values ≥10% were included in further analysis. Finally, the median of the means of the CpG loci identified was plotted against the log-value of the difference in gene expression between tumor and normal tissues for each gene. R (version 3.1.1) was used for calculations and preparing graphs.

Cell lines and culture conditions

Human lung adenocarcinoma cell lines A549, H1975 and SK-MES1 were purchased from ATCC. A549 and H1975 were authenticated with Multiplex human Cell line Authentication Test (Multiplexion, Germany). SK-MES1 cells were used within 6 months after purchasing from the cell bank. All cells were grown in a humidified atmosphere with 5% CO_2 at 37°C. All NSCLC cell lines as well as human primary AECII cells and Phoenix ampho packaging cell line (50) were cultivated in Dulbecco's modified Eagle's Medium (DMEM, Lonza) supplemented with 10% FCS (Gibco) and 1% penicillin/streptomycin (Gibco). For the green fluorescence protein (GFP)-expressing and BAMBI-GFP-expressing cell lines A549 and H1975 1 µg/ml puromycin (Sigma) was added. As a starvation medium DMEM without phenol-red (Lonza) supplemented with 1 mg/ml BSA (Sigma), 1% penicillin/streptomycin (Gibco) and 1% L-Glutamin (Gibco) was used.

DNA transfection

Human BAMBI-GFP insert was obtained from the plasmid pCMV6-AC-GFP (RG200195, OriGene) using BamHI/Pme I restriction sites. The insert was re-cloned into the retroviral expression vector with a Tet-inducible promoter pMOWSIN-TREt (50). As a control pMOWSIN-TREt-GFP was used. Both pMOWSIN-TREt-BAMBI-GFP and pMOWSIN-TREt-GFP were used in combination with pMOWS-rtTAM2 encoding the cDNA for transactivator protein (51). Transfection of the Phoenix ampho packaging cell line was performed by calcium phosphate precipitation. Transducing supernatants were generated 24 h after transfection by passing through a 0.45-µm filter, supplemented with 8 µg/ml polybrene (Sigma) and applied in the proportion 1 : 3.5 (pMOWS-rtTAM2 : pMOWSIN-TREt-BAMBI-GFP or pMOWSIN-TREt-GFP) for spin infection of 1.5×10^5 A549 and H1975 cells. Stably transduced A549 and H1975 cells expressing GFP-tagged human BAMBI or as a control only GFP were selected in the presence of 1.0 µg/ml puromycin (Sigma) 48 h after transduction.

siRNA transfection

siRNA against human BAMBI was purchased from Dharmacon (#LU-019596-00-0002). A549 and SK-MES1 cells were transfected with Lipofectamine RNAiMAX (TheroFisher Scientific, #13778150) according to manufacturer's procedures. Briefly, cells were trypsinized, mixed with required amount of Lipofectamine/siRNA mixture, incubated for 5 min and plated in penicillin/streptomycin-free medium. 12 hours after siRNA transfection, medium was replaced with antibiotic-containing DMEM. Cells were used for TGF-β stimulation 36 hours after siRNA transfection.

Immunoprecipitation and quantitative immunoblotting

For experiments A549, H1975 and SK-MES1 cells were cultivated in growth factor (GF)-depleted medium for 24 h and treated with TGF-β stimulation (R&D Systems) for indicate time periods or left untreated, and then lysed. Before lysis 1 ml of cell supernatant was removed for further analysis by Multiplex bead-based assay (BioRad).
Prior to experiments all cell lines overexpressing GFP or BAMBI-GFP were treated with DOX (5 µg/ml, Sigma) for 24 h and then transferred into starvation medium supplemented with 1.0 µg/ml puromycin (Sigma) and DOX (5 µg/ml, Sigma) for further 24 h.
For lysis cells were scraped in 500 µl lysis buffer (1% NP40, 150 mM NaCl, 20 mM Tris–HCl pH 7.4, 10 mM NaF, 1 mM EDTA pH 8.0, 2 mM $ZnCl_2$ pH 4.0, 1 mM $MgCl_2$, 2 mM Na_3VO_4, 20% glycerol, 2 µg/ml aprotinin and 200 µg/ml AEBSF). Lysates were rotated for 30 min at 4°C and centrifuged for 10 min at 14,000 rpm and 4°C. Protein concentration was

determined by BCA assay and 50 µg of the lysates were used for total cell lysates (TCL) and 750 µg for immunoprecipitation (IP). For IP the antibodies against SMAD2/3, SMAD2, SMAD3 or SMAD4 (BD 610843, Cell Signaling Technology, clone D43B4; clone C67H9; #9515 respectively, dilution 1:100) and Protein A sepharose (GE Healthcare) were added and rotated over night at 4°C. TCLs and immunoprecipitated proteins were separated by SDS-PAGE, transferred to PVDF (TCLs) and nitrocellulose (IP) membranes and immunoblotting was performed with anti-SMAD2/3 (BD 610843), anti-SMAD4 (Cell Signaling Technology, #9515), anti-SMAD7 (R&D, clone 293039), anti-pSmad2 (Cell Signaling 138D4), anti-pSMAD3 (Cell Signaling Technology, clone C25A9), anti-BAMBI (Sigma, HPA010866) and anti-GFP (Roche, clones 7.1 and 13.1) antibodies. Blots probed with anti-pSMAD2 or anti-pSMAD3 antibodies were stripped by using the stripping buffer (6.25 ml 1mMTris pH 6.8, 20 ml 10% SDS, 0.7 ml β-Mercaptoethanol) for 20 min at 65°C and subsequently re-probed with antibodies against total proteins. For all primary antibodies 1:1000 dilution was used. Horseradish peroxidase conjugated goat anti-rabbit (Dianova, 111-035-144) and goat anti-mouse (Dianova, 115-035-146) were used for Enhanced Chemiluminescent (ECL) detection (GE Healthcare). IRDye infrared dyes (LI-COR #926-32211 and #926-68070) secondary antibodies were used for detection with infrared Odyssey imager (LI-COR). Signal quantification was performed using an ImageQuant system (GE Healthcare). Replicates of dose response data were scaled and averaged using methods described in (52).

In vitro cell migration assay

For 2D migration assay H1975 cells overexpressing BAMBI-GFP and GFP were seeded in 24-well plate (Zell Kontakt # 3231-20) at a density of 5,000 cells/well. Cells were allowed to attach for 18 h, after that 5 µg/ml DOX (Sigma) was added into the culture medium. After 48 h cells were serum-starved for 3 h and stimulated with 0.25 ng/ml TGF-β (R&D Systems). After 18 h of stimulation, cells were stained with Hoechst (Sigma) and imaged on an environment-controlled microscope (IX81, Olympus). Images were acquired with an UPlanSApo 10×/0.4 NA objective lens (Olympus) in 15 min intervals for 22 h. Nine positions per well (3×3 grid) were imaged and stitched with ImageJ plugin. Single cell tracking was performed with ImageJ Mtrack2 plugin. Speed of each tracked cell was calculated by dividing total travelled distance by total time, for which cell was tracked. Persistence was calculated by dividing the distance between the first and the last point, where the cell was tracked, by total travelled distance. Resulting number was multiplied by the square root of time, for which cell was tracked divided by maximal possible tracking time, in order to penalize cells, which were tracked for a shorter period of time.

3D collagen invasion assay

3D collage gels were prepared as described previously (53). Briefly, ice-cold 1 M HEPES buffer, 0.7 M NaOH, 10× PBS pH 8.0 and bovine skin collagen G solution (L1613, Biochrome) were mixed in 1:1:2:16 ratio respectively. 50 µl of the resulting solution was added per well of 96-well plate with a flat bottom (BD #353376). A plate was kept overnight at 4°C and then for least 1 h at 37°C to allow gelation of the collagen. After gelation, 10,000 cells per well were seeded on top of the matrix. Expression of GFP or BAMBI-GFP in H1975 cells was induced with 5 µg/ml DOX. 24 hours after DOX induction, cells were stimulated with 0.25 ng/ml TGF-β and left for invasion for 96 h. SK-MES1 cells were siRNA transfected and seeded on a gel. 36 hours after transfected cells were stimulated with 1 ng/ml TGF-β and left for invasion for 96 h. Afterwards, cells were fixed in 3.7% PFA for 1 h and

subsequently stained with Hoechst (Sigma). Collagen embedded cells were imaged using LSM710 confocal microscope (Carl Zeiss) equipped with EC Plan-Neofluar DIC 10×/0.3 NA objective lens (Carl Zeiss). For each well 2×2 tile z-stack was acquired. Image analysis was performed using Imaris software (Bitplane). Spots detection algorithm was applied to assign a spot for fluorescent intensity of each individual nucleus. Resulting spots were filtered by their z-position to separate collagen invaded cells from the cells remained on top of the matrix. Percentage of invaded cells was calculated and used as output.

Lung colonization assay of A549-GFP and A549-BAMBI-GFP cells in nude mice

Animal care and animal experiments were performed according to the national guidelines and were reviewed and confirmed by an institutional review board/ethics committee headed by the local animal welfare officer of the German Cancer Research Center Heidelberg, Germany. All experiments were in accordance with the approved guidelines of the responsible national authority, the local Governmental Committee for Animal Experimentation (Regierungspräsidium Karlsruhe, Germany, license G193/10). Mice were maintained at a 12 hour light-dark cycle with unrestricted diet and water. Two million A549-GFP and A549-BAMBI-GFP cells in 100 µl of PBS were intravenously (i.v.) injected into the lateral tail vein of 7-8 week old female NMRI nu/nu mice purchased from Charles River (Sulzfeld, Germany) and kept on Kliba diet 3307 with n = 12 randomized mice/group. Three days prior to cell inoculation, treatment of all mice with 5 mg/ml doxycycline (DOX) (Sigma, Munich) in drinking water containing 5% saccharose, was started and continued throughout the experiment. TGF-β was injected i.p. (4 µg/kg bodyweight, dissolved at 400 ng/ml in 4 mM HCl containing 0.1% mouse serum albumin, 10 µl/g mouse) once daily at days 1, 6, 11, and 16 post cell inoculation. Prior to cervical dislocation on day 70 post cell inoculation, blood was collected under isoflurane inhalation anesthesia (1-1.5% in O_2, 0.5 l/min) from the *retrobulbar plexus*. No mice were lost due to adverse effects of TGF-β.

Mouse lung colonization assay analysis

Mouse lungs were dissected and separated into left and right lung and subsequently HOPE-fixed and processed as described above. All lung tissue specimens were randomly cut and mounted on SuperFrost slides for hematoxylin and eosin (H&E) staining. For the quantification of the lung tumor burden, the right and left lung of each animal were analyzed by histology-trained investigators (TG, SM) and images were taken at 10× magnification. The area of tumors within the lungs was manually tagged within the Infinity Analyze software (Lumenera, Ottawa, Canada) and tumor area per animal was quantified using a calibrated micrometer slide. The total area of lung tumor burden was calculated from the sum of individual tumor nodule areas within the alveolar region of both lungs from each animal. To calculate the metastatic potential of A549-GFP and A549-BAMBI-GFP cells we manually counted tumor nodules that consisted of at least two connected tumor cells. Human origin of lung tumor cells within the mouse lungs was verified via immunohistochemistry using rabbit anti human HLA-A antibody (clone EP1395Y, Abcam, Cambridge, UK). The expression of the human transgene was confirmed by qRT-PCR (Supplementary Fig. S10). Activation of the TGF-β pathway within human lung tumor cells was investigated by immunohistochemical analysis of SMAD3 phosphorylation.

Assessing *GFP* and *BAMBI-GFP* expression in mice lungs

To investigate the inducible expression of GFP or BAMBI-GFP in our animal experiments, total RNA was extracted from HOPE-fixed, paraffin-embedded tissues as described elsewhere. DNA was digested with DNAse I (Thermo Fisher Scientific) and 200-800 ng of cDNA synthesized with the Maxima First Strand cDNA synthesis Kit (Thermo Fisher Scientific) according to manufacturer`s instructions. Oligonucleotides that target either GFP from A549-GFP control cells (Gene Bank Acc. No. U50963.1) or the GFP sequence from donor vector that was used for cloning BAMBI-GFP (pCMV RG200195 7.3; OriGene) were generated using the Probe Finder software (Roche Applied Science) with default options and normalized to expression of human RPL32 gene via qRT-PCR using the Roche Probes Master Mix and Universal Probe library according to manufacturer`s instructions with 45 cycles of amplification on a Roche LightCycler 480 II (5 min: 95°C Hot Start; 10 s 95°C denaturation and 30 s 60°C annealing). Advanced relative quantification was used to display relative expression normalized to RPL32 as reference gene.

Statistics

Results are shown as means ± SD. Comparisons of datasets were performed using unpaired *t*-test (test group compared to control group). For experiments with human material two-sided paired *t*-test was used to compare the samples groups (tumor to tumor-free). Comparison of SMAD2/3 activation in stably transduced cells was performed using two-way ANOVA with repeated measurements. Otherwise the Mann-Whitney rank sum test was used.

RESULTS

Activation of the TGF-β pathway in human lung cancer tissues

To examine the status of the TGF-β signaling pathway in lung cancer, we employed immunohistochemistry (IHC) to monitor key components of TGF-β signaling in tissues from 133 lung cancer patients with adenocarcinomas (Fig. 1A) and squamous cell carcinomas (Fig. 1B) and in 23 tumor-free lung samples (Fig. 1C). Out of those tumor-free specimens, four (17.4%) were matched samples for NSCLC lung cancer tissues. We analyzed the presence of TGF-β signaling components (Fig. 1D) in both lung cancer cells and compared the expression to type II alveolar epithelial cells (AECII) of the tumor-free tissues. This cell type is considered to be a possible origin of adenocarcinomas (16) and has been recently discussed to exhibit features of progenitor cells (17).

The TGF-β ligand was detected in the majority of the lung cancer tissues (85%) but only in 34.7% of the AECII from the tumor-free samples. Weak staining for SMAD2 and SMAD3 was observed in 22.6% and 11.3% of the lung cancer samples, respectively, whereas in the AECII, SMAD3 was not detectable by means of IHC, and SMAD2 was present in 17.4% of the samples. Immunoblot analysis confirmed 25 times lower abundance of SMAD3 than SMAD2 in isolated populations of AECII cells (Supplementary Fig. S9). For the majority of the lung cancer samples, phosphorylation, indicative of pathway activation, was observed with SMAD2 (78.2%) and SMAD3 (87.2%). In contrast to this, phosphorylation was only present at low levels in 17.3% of the examined AECII. SMAD4 was widely expressed in the lung cancer cells (71.4%) and AECII (60.8%), and SNON (SKI novel protein) was detected in the cytoplasm of almost all the lung cancer specimens (98.5%) as well as in the AECII (87%). Protein expression of the negative regulator SMAD7, a direct target gene of TGF-β signaling, was detected in almost all the lung cancer samples (99.2%) and was primarily localized in nuclear regions. In the AECII, SMAD7 was only moderately expressed (34.8%). Surprisingly, the protein expression of an additional negative regulator of TGF-β signaling, the TGF-β pseudo-receptor BAMBI, was almost completely absent from the lung cancer tissues (1.5%) but frequently detected in the AECII (30.4%). As assessed by Fisher's exact test, a statistically significant difference in the protein expression of TGF-β, pSMAD2, pSMAD3, SMAD3, SMAD7, SNON and BAMBI was observed in the lung cancer cells compared to the AECII (Supplementary Table 1). Furthermore, the frequency of pathway activation, as indicated by the presence of pSMAD2 and pSMAD3 in the same sample, was significantly higher ($p \leq 0.001$) in the lung cancer tissues compared to the tumor-free lung tissues (Supplementary Fig. S1A). No significant differences were observed between adenocarcinomas and squamous cell carcinomas ($p = 0.0549$) (Supplementary Fig. S1B); however, a tendency cannot be neglected. IHC scoring of the four matched tumor-free and NSCLC lung cancer tissues showed a similar trend as the analysis of the entire sample set (Supplementary Table 2).

Differential expression of TGF-β regulated genes in human lung cancer and tumor-free lung tissues

The observed increased activation of TGF-β signaling in lung cancer suggested concomitant alterations at the transcriptional level. Therefore, we analyzed the transcriptome of 19 matched pairs of tumor-free lung tissues and macro-dissected lung NSCLC tumors with Agilent Human Gene Expression arrays. An *a priori*-generated list of genes encoding TGF-β

core pathway members as well as up- and downstream acting mediators (Supplementary Table 2) was used as an input file for the statistical analysis of differentially expressed genes. A paired *t*-test revealed distinct differences between the lung tumors and matched tumor-free tissue samples, and the results were clustered hierarchically and displayed as a heat map (Fig. 2A and Supplementary Table 5). We observed that some genes were up-regulated in all the lung tumor samples compared to the tumor-free tissues, including regulators of the EMT (*SPP1, ADAM12*) and regulators of invasion and metastasis (*RUNX2, RHOA*) (Fig. 2A and Supplementary Table 5). Furthermore, certain genes encoding core components of the TGF-β signaling pathway, *TGFBR2*, *SMAD7* and *BAMBI* (Fig. 2B), were significantly down-regulated in the lung cancer tissues. For BAMBI, the down-regulation of its mRNA corresponded well with the reduced expression of the BAMBI protein in the lung cancer samples (Fig. 1). The divergence between SMAD7 mRNA and protein levels might be due to differences in post-translational regulation in tumor and healthy tissue. Possibly, since SMAD7 mRNA is targeted by multiple miRNAs (18, 19), protein translation of SMAD7 mRNA is inefficient in healthy tissue or proteasomal degradation of SMAD7 mediated e.g. by the E3 ubiquitin ligase Cbl (20) might be impaired in lung cancer cells resulting in elevated SMAD7 protein levels despite reduced mRNA expression. No significant differences between the tumor and tumor-free samples were observed for the intracellular signaling mediators *SMAD2*, *SMAD3*, *SMAD4* or *SNON* (Fig. 2B). The results of the microarray analysis were validated with quantitative Real-Time-PCR (qRT-PCR) (Fig. 2C, Supplementary Fig. S2). Overall, we observed significant alterations in the transcription of TGF-β pathway members and mediators in lung cancer. In line with the absence of the BAMBI protein from lung cancer, we identified distinct differences in the *BAMBI* mRNA expression patterns between tumor-free and tumor lung tissues, indicating a potential role of BAMBI in lung cancer progression.

Methylation patterns of TGF-β pathway members are distinct between lung tumor and tumor-free tissues

Changes in epigenetic modifications are observed during carcinogenesis (21) and have been associated with altered gene expression in tumors. To determine the methylation patterns of TGF-β pathway members and mediators in lung cancer, we examined lung cancer and matched tumor-free tissue samples using Illumina's BeadChip technology. The list of TGF-β core pathway members that was used for the transcriptome analysis (Supplementary Table 2, see Supplementary Table 3 for the raw data) was again utilized to select CpG loci located in the genes of TGF-β pathway members. The selected loci were included in unsupervised hierarchical clustering (Fig. 3A) and principal component analyses (PCA) of DNA methylation values (Fig. 3B). In both analyses, the tumor and tumor-free samples displayed strikingly different methylation patterns. Notably, in 21 of the 26 genes with differences of ≥10% in the median DNA methylation, changes in the DNA methylation between the tumor and tumor-free samples inversely correlated with gene expression (Fig. 3C). For example, the reduced expression of *BAMBI* mRNA corresponded to increased methylation. Based on the reduced expression of BAMBI mRNA and protein in the lung cancer samples, we examined epigenetic modifications of the CpG loci located in the *BAMBI* gene region. Analysis of the 11 loci covered by the HumanMethylation450k BeadChips revealed differential methylation (Fig. 3D, E) between the cancer samples and matched tumor-free lung tissues. Bisulfite pyrosequencing and HumanMethylation450K BeadChip analysis showed similar methylation

patterns of loci located in the *BAMBI* gene region with a Pearson Correlation Coefficient of r = 0.958 (Supplementary Fig. S6). Based on these results, we suggest that major changes in the DNA methylome occur in lung cancer in the genes encoding TGF-β pathway members and mediators. We hypothesized that the epigenetic silencing of the negative regulator of TGF-β signaling BAMBI could alter the signaling cascade to a more activated state and hence influence downstream processes such as TGF-β-dependent EMT.

Differential expression of EMT markers in human lung cancer and tumor-free lung tissues

Therefore, we re-examined our microarray analysis of paired lung cancer and tumor-free tissue samples for the differential expression of EMT markers. With a text-mining search, we generated a list of genes involved in EMT that included genes regulated by TGF-β as well as TGF-β-independent EMT genes (Supplementary Table 2, Supplementary Table 4 and Fig. 4A). Notably, a heterogeneous expression pattern of the mRNAs for EMT mediators was observed (Fig. 4A). *CDH1* (E-cadherin), *MMP9*, *SPP1* (Osteopontin), *HMGA1*, *TWIST1* and *SOX4,* among others (Supplementary Table 5), were significantly up-regulated in lung tumor tissues compared to matched control samples. By contrast, classical EMT-inducing transcription factors, such as *ZEB1, ZEB2,* and *SNAI1*, and structural components associated with the mesenchymal phenotype, such as alpha-smooth muscle actin (*ACTA2*) and Vimentin (*VIM*), exhibited reduced levels of mRNA expression in lung cancer samples (Fig. 4). Validation experiments were performed via qRT-PCR assays (Fig. 4C) and, as revealed in Supplementary Fig. 2, confirmed the results of the transcriptome analysis. The studies further showed that the differential expression of *CDH1*, *SPP1*, *VIM* and *ZEB1* was comparable in adeno- and squamous cell carcinomas, whereas for *CDH2* and *SNAI2*, down-regulation was primarily observed in adenocarcinomas (Fig. 4C).
To analyze the EMT-related alterations at the protein level, we examined the presence of E-cadherin (*CDH1*), N-cadherin (*CDH2*), and Osteopontin (*SPP1*) in the tumor sample cohort (*n* = 130) via immunohistochemistry (Fig. 5A, Supplementary Fig. S3 for representative staining). Again, the tumor samples displayed a mixed phenotype with a high frequency of E-cadherin (90.4%), N-cadherin (93.8%) and Osteopontin (76.9%) protein expression. The AECII from the tumor-free samples displayed a constant expression level of E-cadherin (90%); however, N-cadherin was present in only 5% of the samples, and no Osteopontin expression was observed. Overall, significant differences were observed between the lung cancer samples and AECII regarding the expression frequencies for N-cadherin and Osteopontin (Supplementary Table 1). Furthermore, within the same individual samples (n = 121-126), double-positive staining for pSMAD3/N-cadherin or E-cadherin/N-cadherin was assessed using immunofluorescence (Fig. 5B) and quantified (Fig. 5C). We observed that the majority of pSMAD3-positive tumors were also positive for N-cadherin (79.4%). Additionally, N-cadherin was frequently observed at the invading front of a tumor (in 76.6% of the analyzed cases; see arrows in Fig. 5B) coinciding with a low E-cadherin signal. Notably, double positivity for both E-cadherin and N-cadherin was a frequent feature of lung cancer (91.7%), which is consistent with the RNA data and in the single-stained IHC sample. In summary, the observed alterations in the expression of EMT markers in lung cancer included major changes in the expression of TGF-β target genes.

Abundance and activation of TGF-β pathway components in NSCLC cell lines

A central alteration of TGF-β signaling pathway observed in lung cancer was the loss of the negative regulator BAMBI. To dissect the consequences of the absence of BAMBI and to assess the contribution to lung cancer progression, it was necessary to establish a suitable cellular model system. Therefore, we examined the expression of BAMBI, TGF-β and several downstream pathway components in the NSCLC cell lines A549 and H1975 with immunohistochemical methods (Fig. 6A and B). Similar to the lung cancer tissue samples, the cell lines showed positive signals for TGF-β, SMAD2, SMAD4, SNON, pSMAD2 and pSMAD3 (Fig. 6A and B). However, in contrast to the lung cancer tissues, SMAD7 was weakly expressed (Score 1) and was only observed in H1975 cells. As in the lung cancer tissues, none of the cell lines expressed the BAMBI protein (Fig. 6A, B). This was confirmed by the observation that the amount of *BAMBI* mRNA was significantly lower in the NSCLC cell lines compared to the levels detected in healthy AECII (Fig. 6C). Additionally, the presence of TGF-β in the supernatants of the NSCLC cell lines was analyzed with a multiplex beads-based assay (Supplementary Fig. S4A). The secretion of inactive TGF-β was detected in the supernatants of the NSCLC cell lines independent of the cultivation conditions. However, in both NSCLC cell lines, the level of active TGF-β was low. The induction of TGF-β signaling in the NSCLC cell lines was analyzed by combining enrichment via immunoprecipitation with subsequent immunoblotting (Supplementary Fig. S4B). Compared to the H1975 cells, higher levels of SMAD2 and SMAD3 proteins were observed in the A549 cells. In both cell lines, basal levels of SMAD2 and SMAD3 phosphorylation were detectable upon growth factor depletion or cultivation in regular growth medium. Yet an increase in the phosphorylation of both SMADs was observed upon TGF-β stimulation (Supplementary Fig. S4B). Taken together, the TGF-β signaling in both NSCLC cell lines closely resembles the behavior in the lung cancer samples, making the cell lines suitable model systems for gaining insights into underlying mechanisms.

Altering BAMBI expression affects TGF-β signaling in NSCLC cell lines

A striking feature of the examined lung cancer samples was the absence of the BAMBI protein as well as its reduced mRNA expression. To obtain insights into mechanisms whereby the loss of BAMBI might contribute to tumor progression, we reconstituted BAMBI expression in the NSCLC cell lines utilizing a retroviral TET-On system that facilitates the inducible expression of BAMBI-GFP or GFP alone. We achieved 20 and 100 times higher BAMBI expression level in A549 and H1975 cells, respectively, compared to AECII cells (Fig. 6D). As shown in Fig. 6E, the reconstitution of BAMBI in the H1975 cells resulted in a considerable decrease in SMAD2 and SMAD3 phosphorylation at all the TGF-β concentrations used for stimulation. In the A549 cells, a decrease in SMAD2 and SMAD3 phosphorylation was observed at low TGF-β concentrations (Fig. 6E, Supplementary Fig. S5A, B). To determine whether the reconstitution of BAMBI alters the transcription of genes, we analyzed the TGF-β-induced mRNA expression of selected EMT markers, such as *CDH1* (E-cadherin), *CDH2* (N-cadherin), and *SNAIL2*, for 48 hours and observed that in both A549 and H1975 cells, the mRNA expression levels of each of the examined genes was markedly reduced in the BAMBI-reconstituted cells (Fig. 6F and Supplementary Fig. S5C). These observations correlated with a major reduction at the protein level detected after 48 hours of TGF-β stimulation (Supplementary Fig. S5C). Additionally, we performed siRNA-mediated *BAMBI* knockdown in the lung adenocarcinoma cell line A549 and the lung squamous cell carcinoma cell line SK-MES1 as they showed intermediate reduction of *BAMBI* mRNA in

comparison to AECII. We were able to achieve 80-90% knockdown efficiency in both cell lines (Supplementary Fig. S7B and S8B). *BAMBI* knockdown resulted in higher SMAD2 and SMAD3 phosphorylation and enhanced target gene expression upon TGF-β stimulation in both, A549 and SK-MES1 cells (Fig. 6G, H, and Supplementary Fig. S7 and S8).

Reconstitution of BAMBI in lung cancer cells leads to reduced invasion and tumor growth

To determine the effects of BAMBI reconstitution on cellular responses, we analyzed the TGF-β-induced migration and invasion of H1975-BAMBI-GFP cells and of H1975-GFP cells as a control. In a 2D migration assay, the TGF-β treatment resulted in increased speed (from 2.5 to 3.3 μm/h) and persistence (from 0.275 to 0.425) of cellular movement in control cells, while in the BAMBI-GFP-reconstituted cells the increase was almost entirely abrogated (Fig. 7A). Furthermore, TGF-β treatment resulted in a three-fold increase of invaded H1975-GFP cells in a 3D collagen invasion assay, while in BAMBI-reconstituted cells such increase was not observed, suggesting that the silencing of BAMBI increased the potential of cells to invade in response to TGF-β stimulation (Fig. 7B). Further, we examined the impact of BAMBI loss-of-function on cancer cell invasion. We performed siRNA-mediated knockdown in the squamous lung cell carcinoma cell line SK-MES1 that harbors higher basal expression of *BAMBI* mRNA than the adenocarcinoma cell line H1975. The *BAMBI* mRNA knockdown in SK-MES1 cells resulted in increased invasion of unstimulated cells and importantly enhanced TGF-β-induced invasion for at least one of the siRNA used (Supplementary Fig. S8D).

To investigate the influence of enhanced *BAMBI* expression on the metastatic potential and tumor forming capacity *in vivo*, both A549-GFP control and A549-BAMBI-GFP cells were injected into the tail veins of nude mice. The mice were kept in the presence of doxycycline (DOX) to ensure the expression of GFP or BAMBI-GFP, and the TGF-β ligand was administrated to facilitate cancer cell invasion. Per group twelve animals were injected and kept for ten weeks unless dropout criteria were observed, and mice were sacrificed earlier. In the GFP group two mice that were sacrificed pre-maturely and two mice that survived until the planned end-point of the experiment, developed histologically-confirmed tumors within the lungs. In the BAMBI-GFP cohort lung lesions were observed in one pre-maturely sacrificed mouse and in three mice that survived until the end-point. Overall four mice per group developed lung cancer. Macroscopic investigations of the dissected lungs showed that A549-BAMBI-GFP mice developed fewer lung lesions compared to A549-GFP mice (Fig. 7C).

Histological diagnosis revealed adenocarcinomas in the lungs of both groups (Fig 7D) and qRT-PCR analysis confirmed the presence of human A549 cells expressing either GFP or BAMBI-GFP (Supplementary Fig. S10). To determine the influence of DOX-induced GFP or BAMBI-GFP expression on the metastatic potential of A549 cells, the total amount of lung tumor nodules per animal was quantified. Mice injected with GFP-expressing A549 cells showed a median of 68.5 (17 minimum, 174 maximum) number of tumor nodules per animal, while in mice injected with A549-BAMBI-GFP cells only 2.5 (1 minimum, 25 maximum) nodules per animal were observed (Fig. 7E). Furthermore, the analysis of the tumor areas per animal showed a median tumor area of 8.4×10^7 μm^2 for A549-GFP injected mice whereas the median tumor area of 2.7×10^6 μm^2 was much smaller for mice harboring A549-BAMBI-GFP. Statistical analysis employing the Mann-Whitney test showed for both analysis

significant differences (*p* values of 0.0295 and 0.0286 for number of nodules and tumor area, respectively) between the mice harboring A549 cells that express the GFP control or BAMBI-GFP (Fig. 7E). This demonstrates that BAMBI reconstitution in A549 cells not only impairs TGF-β-induced cancer cell invasion *in vitro* but also *in vivo*. Additionally, immunohistochemical analysis of the human lung tumors within the mouse lungs showed reduced levels of SMAD3 phosphorylation in A549-BAMBI-GFP cells compared to A549-GFP control cells (Fig. 7D) indicating that reconstitution of BAMBI expression also suppressed the activation of TGF-β signaling *in vivo.*

DISCUSSION

In general, the TGF-β signaling cascade is viewed as a double-edged sword in the context of carcinogenesis. At pre-malignant stages this pathway favors anti-proliferative and pro-apoptotic responses. However in advanced tumors TGF-β mediated immunosuppression and enhancement of invasion promote metastatic spread (7). In lung cancer, high TGF-β serum levels correlate with a poor prognosis, lymph node metastasis and tumor progression (22). Furthermore, the expression of TGF-β was an independent risk factor for the occurrence of pulmonary metastasis in NSCLC (23).

We presented a comprehensive in-depth analysis of the status of the TGF-β signaling pathway in lung cancer tissues and discovered a distinct role of the TGF-β pseudo-receptor BAMBI. Strikingly, in almost all the lung cancer tissue samples examined, the negative regulator of TGF-β signaling BAMBI was absent. In line with this observation abundant activation of the TGF-β signaling pathway, indicated by the phosphorylation of both R-SMADs, was observed. On the contrary, in colon carcinomas mutations in TGFBR2 (24) and SMAD4 (25) are frequently observed resulting in the deactivation of signaling pathway. In NSCLC mutations in the receptor (26), the intracellular signal mediators SMAD2 (27) or SMAD4 (28) are rare. Therefore NSCLC seem to retain a functional and active signaling cascade as discussed for breast cancer (7) suggesting a similar role of TGF-β in the carcinogenesis of both types of carcinoma. Currently the role of negative regulator BAMBI in various cancers is controversially discussed. Increased BAMBI expression has been reported for colorectal cancer tissues (11, 13) and ovarian cancer cells (12). In contrast, BAMBI was observed to be epigenetically silenced in high-grade bladder cancer (14) and absent in metastasizing melanoma cells (29) and breast cancer tissues (15). Our results showed that in lung cancer tissues different from matched tumor-free controls, both BAMBI mRNA and protein were absent. The silencing of BAMBI apparently contributes to malignant development, tumor progression and invasion (14, 29).

We hypothesize that the down-regulation of BAMBI sensitizes lung cancer cells to TGF-β and thereby promotes EMT-dependent malignant processes. Central role of TGF-β signaling in EMT regulation has been already observed in breast cancer (30) and esophageal cancer (31). For lung cancer it has been shown that long term TGF-β treatment induces EMT transition in A549 and LC31 lung cancer cell lines (32). Furthermore, Prudkin et al. observed that the EMT phenotype is commonly expressed in primary squamous cell carcinoma and adenocarcinoma of the lung (33). Our studies revealed that BAMBI-negative lung cancer tissues display a mixed EMT phenotype involving the retained expression of epithelial marker proteins (E-cadherin) along with mesenchymal marker proteins (N-cadherin) and EMT-associated markers such as HMGA1 (34) and Osteopontin (*SPP1*) (35). This is in line with the observation that in some metastatic cancers partial EMT is observed (36). It has been proposed that EMT is a highly dynamic and reversible multi-step process. The mixed expression of both epithelial and mesenchymal markers within human lung tumor tissues suggests that, in lung cancer, EMT is only required for a limited time-frame to seed metastases, for example, or that EMT occurs primarily at the invading front of tumors and hence only active at the time of invasive behavior. This possibility is supported by the findings from the immunohistochemistry and immunofluorescence data wherein SPP1 and N-cadherin are observed at the invading front of tumor cells. The EMT program has been linked to chemotherapy resistance in ovarian carcinomas (37) and it has been reported for the A549 lung cell line that chemo-resistance in this cell line was associated with TGF-β-induced EMT

(38). We showed that the restoration of BAMBI expression in NSCLC cell lines reduced TGF-β induced phosphorylation of the R-SMADs. As a consequence TGF-β mediated expression of EMT markers was markedly attenuated and the induction of cell migration and invasion was significantly reduced. Furthermore, the *in vivo* experiments strongly suggest a pivotal role of BAMBI with regard to tumor growth and metastasizing capability. These observations identify BAMBI as a negative regulator of TGF-β-induced EMT responses in NSCLC and suggest a role for BAMBI as a tumor suppressor in lung cancer.

Our epigenetic analysis reveals severe alterations in the DNA methylation patterns of TGF-β signaling pathway genes in lung cancer. Accordingly, aberrant DNA methylation of TGF-β signaling pathway genes was observed in gastric adenocarcinoma (39), showing that the methylation frequency of TGFBR1 and TGFBR2 in the tissues of high grade dysplasia and GCA was significantly elevated and associated with mRNA and protein expression of the two genes. Further, more frequent TGFBR1 and TGFBR2 promoter hypermethylation was detected in stage III and stage IV esophageal squamous cell carcinoma tissue indicating that promoter methylation of TGFBR1 and TGFBR2 may exist in the early stage of ESCC and play important roles in TGFBR1 and TGFBR2 gene silencing (40). In rat prostate cancer cell lines treatment with demethylating agent, 5-aza-2'-deoxycytidine resulted in upregulation of several genes including TGFBR2 and epigenetic silencing of TGFBR2 gene was observed in high-grade prostatic intraepithelial neoplasia (41). Cheng et al. showed that epigenetic silencing of SMAD8 expression by DNA hypermethylation in breast and colon cancers directly correlated with loss of SMAD8 expression (42). These findings not only underline the impact of alterations in the DNA methylation pattern of TGF-β pathway genes in numerous cancer types but also support our conclusion that aberrant DNA methylation might affect the activity of the TGF-β pathway in lung cancer.

The in-depth analysis of patient samples and mechanistic insights from *in vitro* studies presented in this report reveal major alterations in the TGF-β-pathway in lung cancer and suggest that this pathway might be a promising therapeutic target. To our knowledge, there are currently no completed clinical trials targeting the TGF-β pathway in lung cancer patients. For other cancer types, it has been shown, for example, that the radiotherapy-induced elevation of TGF-β serum levels in a mouse model of breast cancer favors metastasis but can be abrogated by TGF-β-targeted antibodies (43). In addition, the targeting of EGFR signaling by the EGFR antibody Cetuximab in a xenograft model of head and neck cancer resulted in emergence of resistant tumor cells that expressed relatively higher levels of TGF-β and elevated levels of TGF-β in the tumor microenvironment enable tumor cells to evade antibody-dependent cell-mediated cytotoxicity (ADCC) and resist the antitumor activity of Cetuximab *in vivo*. These results show that TGF-β is a key molecular determinant of resistance of cancers to EGFR-targeted therapy (44).

A recent study identified MED12, a component of the transcriptional MEDIATOR complex that is mutated in cancers, as a determinant of response to ALK and EGFR inhibitors. Similar to BAMBI, MED12 negatively regulates TGF-β receptor through physical interaction and its suppression results in activation of TGF-β signaling, which is both necessary and sufficient for drug resistance. MED12 loss induces an EMT-like phenotype, which is associated with chemotherapy resistance in colon cancer patients and to gefitinib in lung cancer (45).

We suggest that in lung cancer epigenetic silencing of BAMBI results in elevated TGF-

β signaling favoring invasion, migration and EMT. Further we speculate that an elevated activation of TGF-β signaling pathway in the absence of the negative regulator BAMBI may enhance the immunosuppressive effects (7) of TGF-β in tumor microenvironment and promote cancer cell invasion. Therefore we propose a central role of altered TGF-β signaling in lung cancer progression.

Acknowledgments & funding:

We thank Jasmin Tiebach, Maria Lammers, Kristin Wiczkowski, Bettina Baron-Lühr, Anna Schiller and Lorena Valles for excellent technical assistance.

The support of Damir Krunic from the DKFZ Light Microscopy facility and of Steffen Schmitt from the DKFZ FACS facility is gratefully acknowledged. We thank Bettina Oerhle and Gerald Burgstaller from Oliver Eickelberg's lab at CPC Munich for their help with establishing the 3D collagen invasion assay. We thank DKFZ Tumor Models core facility for support with *in vivo* mouse experiments.

This study was funded by the German Center for Lung Research [Deutsches Zentrum für Lungenforschung (DZL)], the German Ministry of Education and Research (BMBF) and in part by the Klara und Werner Kreitz Stiftung (SM). We also acknowledge funding from the BMBF within the CancerSys network "LungSys II" and Virtual Liver Network and funding by an NIH grant 1R01DK090347-01. Magdalena Szczygieł was supported by the Helmholtz International Graduate School for Cancer Research at the German Cancer Research Center (DKFZ).

Patient tissues were provided by the BioMaterialBank North, which is funded in part by the Airway Research Center North (ARCN), Member of the German Center for Lung Research (DZL) and is member of popgen 2.0 network (P2N) which is supported by a grant from the German Ministry for Education and Research (01EY1103).

Author contributions:

TG conceived the study of the tissue samples, and UK conceived the mechanistic analysis in the NSCLC cell lines. TG and UK supervised the project. The immunohistochemistry and microarray analysis were performed by SM. HM supervised the preparation and cultivation of the AECII. The measurement of mRNA levels via qRT-PCR assays was conducted by SD, RM and SM. The immunoblotting experiments were conducted by DD, RM and PL. The retroviral transduction and BAMBI reconstitution were performed by SD. MS performed 3D invasion experiments in squamous cell lines. DD performed siRNA BAMBI knockdowns and evaluated their effects in biochemical assays. The invasion and migration experiments for H1975 cells were conducted by DD. KMD, DD and UK designed *in vivo* mouse experiments. SM processes and analyzed the mouse tissues. OA, RS, SS and MK performed DNA methylation analyses and analyzed the data; KFR was responsible for the pneumology, MR for the oncology, EV for the pathology and CK for the surgical aspects. SM, SD, DD, HM, UK and TG wrote the manuscript, and all the authors approved the manuscript.

Reference List

1. Ferlay J, Shin HR, Bray F, Forman D, Mathers C, Parkin DM. Estimates of worldwide burden of cancer in 2008: GLOBOCAN 2008. Int J Cancer. 2010;127:2893-917.
2. Morgensztern D, Ng SH, Gao F, Govindan R. Trends in stage distribution for patients with non-small cell lung cancer: a National Cancer Database survey. J Thorac Oncol. 2010;5:29-33.
3. Siegel R, Naishadham D, Jemal A. Cancer statistics, 2012. CA Cancer J Clin. 2012;62:10-29.
4. Pain M, Bermudez O, Lacoste P, Royer PJ, Botturi K, Tissot A, et al. Tissue remodelling in chronic bronchial diseases: from the epithelial to mesenchymal phenotype. Eur Respir Rev. 2014;23:118-30.
5. Hugo H, Ackland ML, Blick T, Lawrence MG, Clements JA, Williams ED, et al. Epithelial--mesenchymal and mesenchymal--epithelial transitions in carcinoma progression. J Cell Physiol. 2007;213:374-83.
6. Siegel PM, Massague J. Cytostatic and apoptotic actions of TGF-beta in homeostasis and cancer. Nat Rev Cancer. 2003;3:807-21.
7. Massague J. TGFbeta in Cancer. Cell. 2008;134:215-30.
8. Moustakas A, Heldin CH. The regulation of TGFbeta signal transduction. Development. 2009;136:3699-714.
9. Onichtchouk D, Chen YG, Dosch R, Gawantka V, Delius H, Massague J, et al. Silencing of TGF-beta signalling by the pseudoreceptor BAMBI. Nature. 1999;401:480-5.
10. Dromann D, Rupp J, Rohmann K, Osbahr S, Ulmer AJ, Marwitz S, et al. The TGF-beta-pseudoreceptor BAMBI is strongly expressed in COPD lungs and regulated by nontypeable Haemophilus influenzae. Respir Res. 2010;11:67.
11. Sekiya T, Adachi S, Kohu K, Yamada T, Higuchi O, Furukawa Y, et al. Identification of BMP and activin membrane-bound inhibitor (BAMBI), an inhibitor of transforming growth factor-beta signaling, as a target of the beta-catenin pathway in colorectal tumor cells. J Biol Chem. 2004;279:6840-6.
12. Pils D, Wittinger M, Petz M, Gugerell A, Gregor W, Alfanz A, et al. BAMBI is overexpressed in ovarian cancer and co-translocates with Smads into the nucleus upon TGF-beta treatment. Gynecol Oncol. 2010;117:189-97.
13. Togo N, Ohwada S, Sakurai S, Toya H, Sakamoto I, Yamada T, et al. Prognostic significance of BMP and activin membrane-bound inhibitor in colorectal cancer. World J Gastroenterol. 2008;14:4880-8.
14. Khin SS, Kitazawa R, Win N, Aye TT, Mori K, Kondo T, et al. BAMBI gene is epigenetically silenced in subset of high-grade bladder cancer. Int J Cancer. 2009;125:328-38.
15. Lang DS, Marwitz S, Heilenkotter U, Schumm W, Behrens O, Simon R, et al. Transforming growth factor-beta signaling leads to uPA/PAI-1 activation and metastasis: a study on human breast cancer tissues. Pathol Oncol Res. 2014;20:727-32.
16. Lin C, Song H, Huang C, Yao E, Gacayan R, Xu SM, et al. Alveolar type II cells possess the capability of initiating lung tumor development. PLoS One. 2012;7:e53817.
17. Borok Z, Crandall ED. More life for a "terminal" cell. Am J Physiol Lung Cell Mol Physiol. 2009;297:L1042-4.
18. Butz H, Racz K, Hunyady L, Patocs A. Crosstalk between TGF-beta signaling and the microRNA machinery. Trends Pharmacol Sci. 2012;33:382-93.
19. Gronroos E, Hellman U, Heldin CH, Ericsson J. Control of Smad7 stability by competition between acetylation and ubiquitination. Molecular cell. 2002;10:483-93.
20. Gruber T, Hinterleitner R, Hermann-Kleiter N, Meisel M, Kleiter I, Wang CM, et al. Cbl-b mediates TGFbeta sensitivity by downregulating inhibitory SMAD7 in primary T cells. Journal of molecular cell biology. 2013;5:358-68.
21. Shen H, Laird PW. Interplay between the cancer genome and epigenome. Cell. 2013;153:38-55.

22. Hasegawa Y, Takanashi S, Kanehira Y, Tsushima T, Imai T, Okumura K. Transforming growth factor-beta1 level correlates with angiogenesis, tumor progression, and prognosis in patients with nonsmall cell lung carcinoma. Cancer. 2001;91:964-71.
23. Saji H, Nakamura H, Awut I, Kawasaki N, Hagiwara M, Ogata A, et al. Significance of expression of TGF-beta in pulmonary metastasis in non-small cell lung cancer tissues. Ann Thorac Cardiovasc Surg. 2003;9:295-300.
24. Grady WM, Willis JE, Trobridge P, Romero-Gallo J, Munoz N, Olechnowicz J, et al. Proliferation and Cdk4 expression in microsatellite unstable colon cancers with TGFBR2 mutations. Int J Cancer. 2006;118:600-8.
25. Jones S, Chen WD, Parmigiani G, Diehl F, Beerenwinkel N, Antal T, et al. Comparative lesion sequencing provides insights into tumor evolution. Proc Natl Acad Sci U S A. 2008;105:4283-8.
26. Anumanthan G, Halder SK, Osada H, Takahashi T, Massion PP, Carbone DP, et al. Restoration of TGF-beta signalling reduces tumorigenicity in human lung cancer cells. Br J Cancer. 2005;93:1157-67.
27. Uchida K, Nagatake M, Osada H, Yatabe Y, Kondo M, Mitsudomi T, et al. Somatic in vivo alterations of the JV18-1 gene at 18q21 in human lung cancers. Cancer Res. 1996;56:5583-5.
28. Nagatake M, Takagi Y, Osada H, Uchida K, Mitsudomi T, Saji S, et al. Somatic in vivo alterations of the DPC4 gene at 18q21 in human lung cancers. Cancer Res. 1996;56:2718-20.
29. Degen WG, Weterman MA, van Groningen JJ, Cornelissen IM, Lemmers JP, Agterbos MA, et al. Expression of nma, a novel gene, inversely correlates with the metastatic potential of human melanoma cell lines and xenografts. Int J Cancer. 1996;65:460-5.
30. Taube JH, Herschkowitz JI, Komurov K, Zhou AY, Gupta S, Yang J, et al. Core epithelial-to-mesenchymal transition interactome gene-expression signature is associated with claudin-low and metaplastic breast cancer subtypes. Proc Natl Acad Sci U S A. 2010;107:15449-54.
31. Ohashi S, Natsuizaka M, Wong GS, Michaylira CZ, Grugan KD, Stairs DB, et al. Epidermal growth factor receptor and mutant p53 expand an esophageal cellular subpopulation capable of epithelial-to-mesenchymal transition through ZEB transcription factors. Cancer Res. 2010;70:4174-84.
32. Pirozzi G, Tirino V, Camerlingo R, Franco R, La Rocca A, Liguori E, et al. Epithelial to mesenchymal transition by TGFbeta-1 induction increases stemness characteristics in primary non small cell lung cancer cell line. PLoS One. 2011;6:e21548.
33. Prudkin L, Liu DD, Ozburn NC, Sun M, Behrens C, Tang X, et al. Epithelial-to-mesenchymal transition in the development and progression of adenocarcinoma and squamous cell carcinoma of the lung. Mod Pathol. 2009;22:668-78.
34. Pegoraro S, Ros G, Piazza S, Sommaggio R, Ciani Y, Rosato A, et al. HMGA1 promotes metastatic processes in basal-like breast cancer regulating EMT and stemness. Oncotarget. 2013;4:1293-308.
35. Alonso SR, Tracey L, Ortiz P, Perez-Gomez B, Palacios J, Pollan M, et al. A high-throughput study in melanoma identifies epithelial-mesenchymal transition as a major determinant of metastasis. Cancer Res. 2007;67:3450-60.
36. Debnath J, Brugge JS. Modelling glandular epithelial cancers in three-dimensional cultures. Nat Rev Cancer. 2005;5:675-88.
37. Latifi A, Abubaker K, Castrechini N, Ward AC, Liongue C, Dobill F, et al. Cisplatin treatment of primary and metastatic epithelial ovarian carcinomas generates residual cells with mesenchymal stem cell-like profile. J Cell Biochem. 2011;112:2850-64.
38. Toge M, Yokoyama S, Kato S, Sakurai H, Senda K, Doki Y, et al. Critical contribution of MCL-1 in EMT-associated chemo-resistance in A549 non-small cell lung cancer. Int J Oncol. 2015;46:1844-8.
39. Guo W, Dong Z, Guo Y, Kuang G, Yang Z, Shan B. Concordant repression and aberrant methylation of transforming growth factor-beta signaling pathway genes occurs early in gastric cardia adenocarcinoma. Mol Biol Rep. 2012;39:9453-62.
40. Dong Z, Guo W, Guo Y, Kuang G, Yang Z. Concordant promoter methylation of transforming growth factor-beta receptor types I and II occurs early in esophageal squamous cell carcinoma. Am J Med Sci. 2012;343:375-81.

41. Yamashita S, Takahashi S, McDonell N, Watanabe N, Niwa T, Hosoya K, et al. Methylation silencing of transforming growth factor-beta receptor type II in rat prostate cancers. Cancer Res. 2008;68:2112-21.
42. Cheng KH, Ponte JF, Thiagalingam S. Elucidation of epigenetic inactivation of SMAD8 in cancer using targeted expressed gene display. Cancer Res. 2004;64:1639-46.
43. Biswas S, Guix M, Rinehart C, Dugger TC, Chytil A, Moses HL, et al. Inhibition of TGF-beta with neutralizing antibodies prevents radiation-induced acceleration of metastatic cancer progression. J Clin Invest. 2007;117:1305-13.
44. Bedi A, Chang X, Noonan K, Pham V, Bedi R, Fertig EJ, et al. Inhibition of TGF-beta enhances the in vivo antitumor efficacy of EGF receptor-targeted therapy. Mol Cancer Ther. 2012;11:2429-39.
45. Huang S, Holzel M, Knijnenburg T, Schlicker A, Roepman P, McDermott U, et al. MED12 controls the response to multiple cancer drugs through regulation of TGF-beta receptor signaling. Cell. 2012;151:937-50.
46. Goldmann T, Dromann D, Marzouki M, Schimmel U, Debel K, Branscheid D, et al. Tissue microarrays from HOPE-fixed specimens allow for enhanced high throughput molecular analyses in paraffin-embedded material. Pathol Res Pract. 2005;201:599-602.
47. Marwitz S, Abdullah M, Vock C, Fine JS, Visvanathan S, Gaede KI, et al. HOPE-BAL: improved molecular diagnostics by application of a novel technique for fixation and paraffin embedding. J Histochem Cytochem. 2011;59:601-14.
48. Marwitz S, Kolarova J, Reck M, Reinmuth N, Kugler C, Schadlich I, et al. The tissue is the issue: improved methylome analysis from paraffin-embedded tissues by application of the HOPE technique. Lab Invest. 2014;94:927-33.
49. Friemel C, Ammerpohl O, Gutwein J, Schmutzler AG, Caliebe A, Kautza M, et al. Array-based DNA methylation profiling in male infertility reveals allele-specific DNA methylation in PIWIL1 and PIWIL2. Fertility and sterility. 2014;101:1097-103 e1.
50. Kinsella TM, Nolan GP. Episomal vectors rapidly and stably produce high-titer recombinant retrovirus. Hum Gene Ther. 1996;7:1405-13.
51. Pfeifer AC, Kaschek D, Bachmann J, Klingmuller U, Timmer J. Model-based extension of high-throughput to high-content data. BMC Syst Biol. 2010;4:106.
52. von der Heyde S, Sonntag J, Kaschek D, Bender C, Bues J, Wachter A, et al. RPPanalyzer toolbox: an improved R package for analysis of reverse phase protein array data. Biotechniques. 2014;57:125-35.
53. Burgstaller G, Oehrle B, Koch I, Lindner M, Eickelberg O. Multiplex profiling of cellular invasion in 3D cell culture models. PLoS One. 2013;8:e63121.

FIGURE LEGENDS:

Figure 1: **BAMBI is absent and the TGF-β signaling pathway is abundantly activated in lung cancer tissues.**

A-C, Detection and localization of TGF-β pathway proteins via immunohistochemistry on HOPE-fixed paraffin-embedded (A) lung adenocarcinomas (*n* = 59 patients), (B) lung squamous cell carcinomas (*n* = 74 patients) and (C) tumor-free lung tissues (*n* = 23 patients). All the images are at 40x magnification with scale bar = 100 µm. Positive staining is indicated by a red color (AEC). For each antibody, a positive signal was observed for at least some of the samples. Representative images are shown for each tumor type and for tumor-free lung tissue.

D, Scoring of expression levels in lung cancer tissues (*n* = 133 patients) and in healthy type II alveolar epithelial cells (AECII) from tumor-free lung tissue (*n* = 23 patients). Bar charts indicate semi-quantitative scores based on the histological analysis of the entire specimen as follows: negative (0), focal and weak expression (1), frequent intermediate expression (2), strong expression and dominating feature of specimen (3). Numbers above the bars display the total positive cases observed overall in percent.

Figure 2: TGF-β-regulated genes are differentially expressed in human lung cancer tissues and tumor-free lung tissues.

A, Nineteen samples of HOPE-fixed paraffin-embedded tissues from matched lung cancer and tumor-free lung samples were macro-dissected and subjected to analysis on Agilent Human Whole Genome Expression arrays. A list of 80 direct and indirect TGF-β pathway members (Supplementary Table 2) as well as up- and downstream acting mediators were used as inputs for gene expression analysis to analyze the transcriptional regulation of this pathway. A heatmap of hierarchical clustering computed with a squared Euclidian distance matrix and Ward`s linkage rule is shown for the significant results from paired *t*-tests of tumor-free lung against matched tumor samples with a Benjamini-Hochberg multiple comparison correction ($p \leq 0.05$). Relative gene expression levels are displayed for individual cases according to the histological tumor entity abbreviated as follows: SQC, squamous cell carcinoma; AC, adenocarcinoma.

B, Quantile-normalized microarray data indicating the expression of TGF-β receptors *TGFBR1* and *TGFBR2*, *BAMBI* and downstream mediators in matched tumor-free lung tissues and lung cancer samples (*n* = 18) compared with a two-sided paired *t*-test with **, $p \leq 0.01$ and ***, $p \leq 0.001$ regarded as significant, n.s. not significant.

C, Validation of the microarray data for individual targets with qPCR assays. Gene expression in tumor-free and tumor samples from the 19 patients. Up-regulated genes are displayed above the black line, which indicates a ratio of 1 (equal expression rates in tumor and tumor-free lung tissues), and down-regulated genes are displayed below this line. Blue dots - squamous cell carcinoma (SQC); red dots - adenocarcinoma (AC).

Figure 3: **Methylation patterns of TGF-β pathway members distinguish between lung tumor and tumor-free tissues**

A-B, DNA methylation analysis of TGF-β pathway member genes in tumor and tumor-free lung tissues. Forty-six samples of macro-dissected, HOPE-fixed and paraffin-embedded tissues were subjected to genome-wide methylome analysis using Illumina's HumanMethylation450K BeadChips. The same *a priori* list of TGF-β pathway members used for the microarray analysis was used to extract DNA methylation values for the CpG loci located in these genes for an unsupervised hierarchical cluster analysis (A) and a principal component analysis (PCA, B). The data were normalized for visualization (mean = 0).

C, Correlation of the DNA methylation and gene expression data for TGF-β pathway member genes differentially methylated between lung cancer and tumor-free lung tissues. Twenty-six TGF-β pathway member genes differentially methylated between lung cancer and tumor-free lung tissues (delta methylation ≥ 10%) and aberrantly expressed in lung cancer samples (≥ 1.5-fold) were identified as described in the Materials and Methods section. The mean differential methylation in all the tumor-control sample pairs was determined for each CpG locus included in the analysis. Subsequently, the median of the means of the CpG loci was calculated for each gene, resulting in one differential DNA methylation value per gene (Δ DNA methylation). The median was plotted against the log-value of the difference in gene expression between the tumor and normal tissues for each gene. Differences in the DNA methylation values between the tumor and tumor-free samples were plotted against the difference in expression (log-value) as determined by the array analysis for each gene. For 21 genes, an inverse correlation between DNA methylation and gene expression (quadrants II and IV) was found. By contrast, DNA methylation directly correlated with gene expression in 5 genes (quadrants I and III).

D-E, Hierarchical cluster analysis and PCA of 11 CpG loci present on the 450k BeadChip and located in the BAMBI gene demonstrated heterogeneous DNA methylation at the BAMBI locus. In the bar on top of the heatmap, red indicates lung adenocarcinoma, blue indicates lung squamous cell carcinoma and black indicates tumor-free lung cancer samples. In the heatmap, blue indicates low DNA methylation values, black indicates intermediate and yellow indicates high DNA methylation values. The data were normalized for visualization (mean = 0).

Figure 4: Differential mRNA expression of EMT markers in human lung cancer and tumor-free lung tissues.

A, EMT genes (supplementary table 4) significantly differentially regulated between macro-dissected lung tumors and matched tumor-free lung tissues (n = 19) were identified from microarray analysis by paired t-testing with a Benjamini-Hochberg multiple testing correction ($p \leq 0.05$). A heatmap of hierarchical clustering was computed with a squared Euclidian distance matrix and Ward`s linkage rule. The relative gene expression level is displayed for individual cases according to the histological tumor type and is abbreviated as follows: SQC, squamous cell carcinoma; AC, adenocarcinoma.

B, Quantile-normalized relative expression levels for single genes in the EMT data set are compared between tumor-free lung tissues and tumor samples using a two-sided paired *t*-test with **, $p \leq 0.01$ and ***, $p \leq 0.001$ regarded as significant, n.s. not significant.

C, Validation of the microarray data for single genes via qRT-PCR assays of paraffin-embedded material depicted as relative expression levels. Gene expression in tumor-free lung versus tumor samples from 18 patients. Up-regulated genes are above and down-regulated genes are below the black line indicating a ratio of 1 (equal expression rates in tumor and tumor-free lung). Blue dots - squamous cell carcinoma (SQC); red dots - adenocarcinoma (AC).

Figure 5: Frequency of EMT markers on protein level differs in human lung cancer and tumor-free lung tissues.

A, Immunohistochemical scoring of paraffin-embedded tumor samples (*n* = 130) and AECII from tumor-free lungs with antibodies recognizing E-cadherin (*CDH1*), N-cadherin (*CDH2*) and Osteopontin (*SPP1*) in squamous cell carcinomas (SQC), adenocarcinomas (AC) and healthy AECII cells. Bar charts: Numbers above the bars display the total positive cases observed overall in percent.
B, Representative images of double-immunostaining with either pSMAD3 (green) and N-cadherin (red) (upper row) or with E-cadherin (green) and N-cadherin (red) (lower row) in the same paraffin-embedded tumor (*n* for each marker = 121-126). Arrows indicate CDH2 expression at the tumor cell invasion front, scale bar = 50 µm.
C, Frequency of different combinations of EMT markers as determined by double immunofluorescence staining (*n* = 121-127) displayed as percentages.

Figure 6: **Altering BAMBI expression affects TGF-β signaling in NSCLC cell lines.**

A, Representative immunocytochemical stainings of the indicated proteins in HOPE-fixed paraffin-embedded NSCLC lung cancer cell lines H1975 and A549. The staining was performed as described for the tissue sections. 40× magnification, scale bar = 50 µm.
B, Scoring of the expression of the indicated proteins in cell lines A549 and H1975. Bar charts indicate no expression (0), focal expression (1), frequent expression (2) or expression as the dominant pattern (3).
C, Relative expression of *BAMBI* mRNA in the indicated lung cancer cell lines in comparison to healthy AECII. The mean ± SD of qRT-PCR determinations from three AECII isolations and from three biological triplicates of the lung cancer cell lines are shown. Statistical analysis was performed using one-way ANOVA test with ***, $p \leq 0.001$ regarded as significant, n.s. not significant.
D, Relative expression of *BAMBI* mRNA in DOX-treated NSCLC cell lines in comparison to healthy AECII. Data represent the mean from four biological replicates ± SD. Statistical analysis was performed using one-way ANOVA test with ***, $p \leq 0.001$ regarded as significant.
E, Quantification of TGF-β dose-dependent phosphorylation of SMAD2 and SMAD3 in H1975-GFP and H1975-BAMBI-GFP as well as in A549-GFP and A549-BAMBI-GFP cells. For each cell line the SMAD2/3 phosphorylation was determined by quantitative immunoblotting. The data shown are the mean of three biological replicates (provided in Supplementary Fig. S5). The shaded area indicates the standard error of the mean. Statistical analysis was performed using two-way ANOVA with repeated measurements and the *p*-values ≤ 0.05 were considered significant.

F, Expression of the indicated EMT genes in H1975 and A549 cell lines stably transduced with GFP or BAMBI-GFP was assessed by qRT-PCR. The GFP and BAMBI-GFP expression was induced with DOX for 48 h, and cells were stimulated with TGF-β (0.1 ng/ml) for the indicated time points. mRNA levels were normalized using the geometric mean of the β-glucuronidase (*GUSB*) and esterase D (*ESD*) housekeeping genes. The experiments were performed in six biological replicates and the data represent mean values ± SD.
G, Quantification of the dynamics of TGF-β induced SMAD2/3 phosphorylation upon *BAMBI* knockdown in A549 and SK-MES1 cells. A549 and SK-MES1 cells were transfected with BAMBI-specific siRNAs or control siRNA for 36 hours (knockdown efficiency is shown in Supplementary Fig. S7 and S8). After stimulation with 1 ng/ml TGF-β for the indicated time SMAD2/3 phosphorylation was determined by quantitative immunoblotting. For each cell line the data shown are the mean of three independent experiments (replicates provided in Supplementary Fig. S7 and S8), and the shaded area indicates the standard error of the mean.
H, Expression of the indicated EMT genes in A549 and SK-MES1 cell lines transfected with BAMBI-specific siRNAs or control siRNA for 36 hours stimulated with 1 ng/ml TGF-β was assessed by qRT-PCR. RNA levels were normalized using the geometric mean of the glyceraldehyde-3-phosphate dehydrogenase (*GAPDH*) and glucose-6-phosphate 1-dehydrogenase D (*G6PD*) housekeeping genes. Data shown represent mean ± SD from three independent experiments.

Figure 7: **Reconstitution of BAMBI expression in lung cancer cells reduces TGF-β-mediated invasion capacity *in vitro* and *in vivo*.**

A, Persistence and movement speed of H1975-GFP and H1975-BAMBI-GFP cells, stimulated with 0.25 ng/ml TGF-β and imaged for 22 h. The box is bound by the 25th and 75th quantiles. The whiskers extend to three-halves of the interquartile range. The lines indicate the median and dots illustrate the 5th and 95th quantiles. Each box contains at least 350 cells from two independent experiments, nine biological replicates in total. Statistical analysis was performed using the Mann-Whitney rank sum test; ***, $p \leq 0.001$.
B, Quantification of the number of H1975-GFP and H1975-BAMBI-GFP cells that invaded into the collagen gel. The data of one representative experiment is shown. Every dot correspond to one biological replicate, black line is the median. A second independent replicate is shown in Supplementary Fig. 5F. Statistical analysis was performed using one-way ANOVA with ***, $p \leq 0.001$ regarded as significant.
C, Representative images of mouse lungs nine weeks after tail vein injection of A549-GFP or A549-BAMBI-GFP cells. Lung macrometastases are indicated with white arrows.
D, Histological analysis of lung tumor burden in mice injected with A549-GFP or A549-BAMBI-GFP. Lung tumor area within the hematoxylin and eosin (H&E) stained tissue section of animal lungs was quantified using Infinity Analyze software. Exemplary images of tissue sections from A549-GFP- and A549-BAMBI-GFP-injected animals are shown and lung tumors are manually marked by black borders (upper panels). Activity of the TGF-β pathway was determined by IHC detection of pSMAD3 (lower panels). All images are taken at 10× magnification with a scale bar of 200 µm.
E, Quantification of human lung tumor nodules and lung tumor areas within animal lungs after tail vein injection of A549-GFP and A549-BAMBI-GFP cells. Tumor nodules were counted on H&E-stained sections from each lung of every animal that developed histology-confirmed lung tumors (n = 4 each). The total area of lung tumor per animal as determined

by image analysis on H&E-stained sections (n = 4 each). All data is displayed as box and whiskers plot showing the median and minimum/maximum. For statistical evaluation of non-parametric data, the Mann-Whitney test (one-tailed) was applied and a p value ≤ 0.05 (*) was regarded as significant.

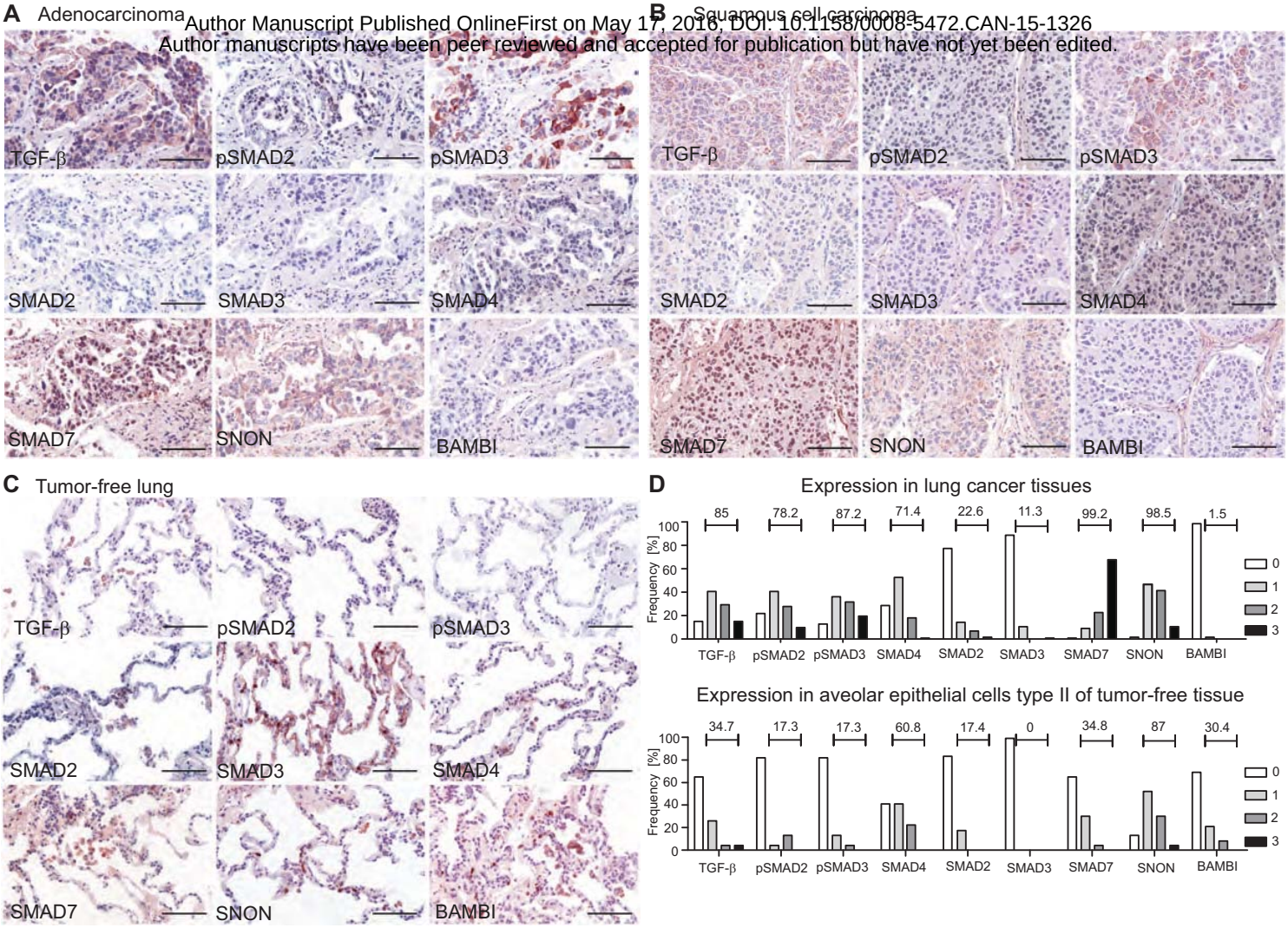

Marwitz et al., Figure 1

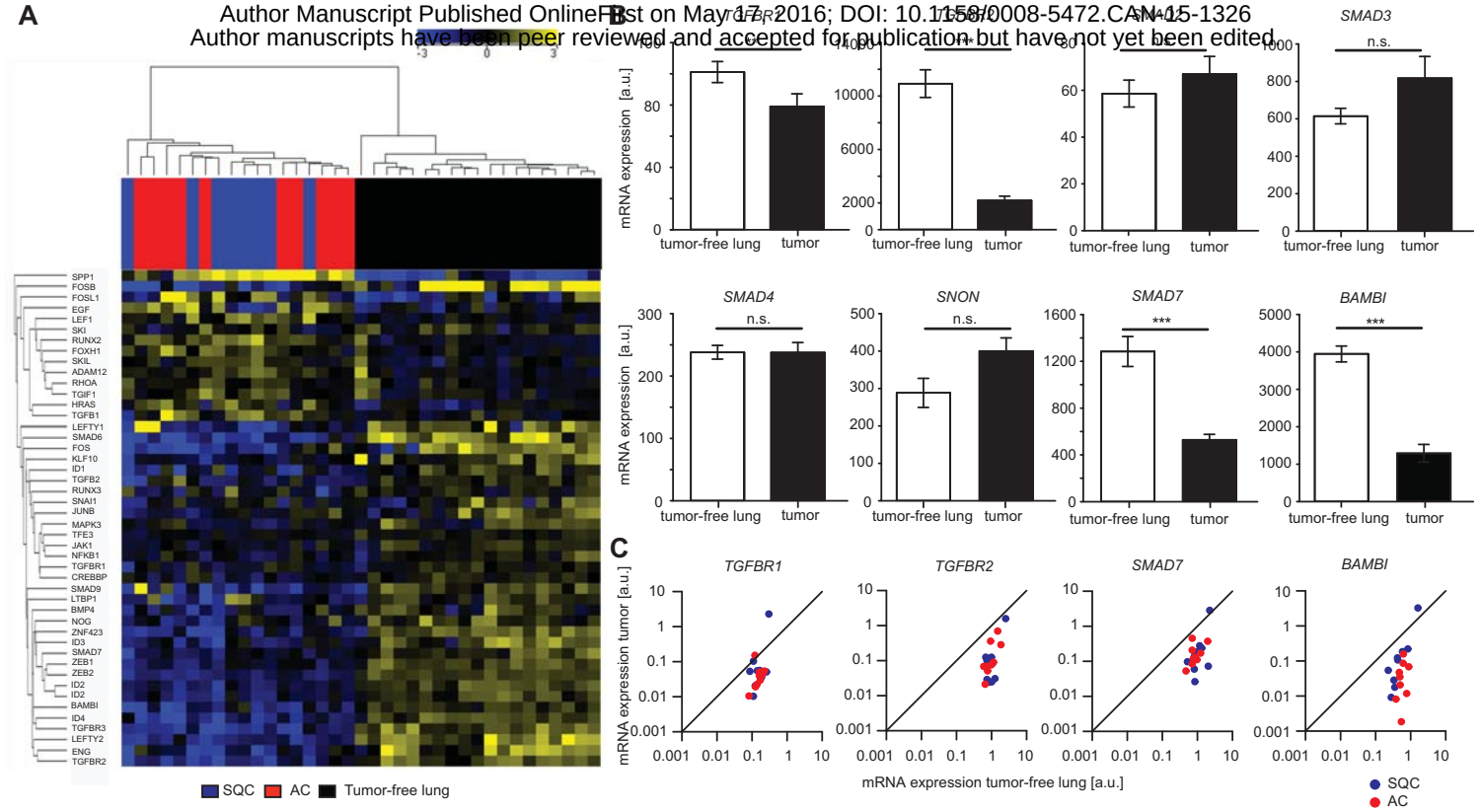

Marwitz et al., Figure 2

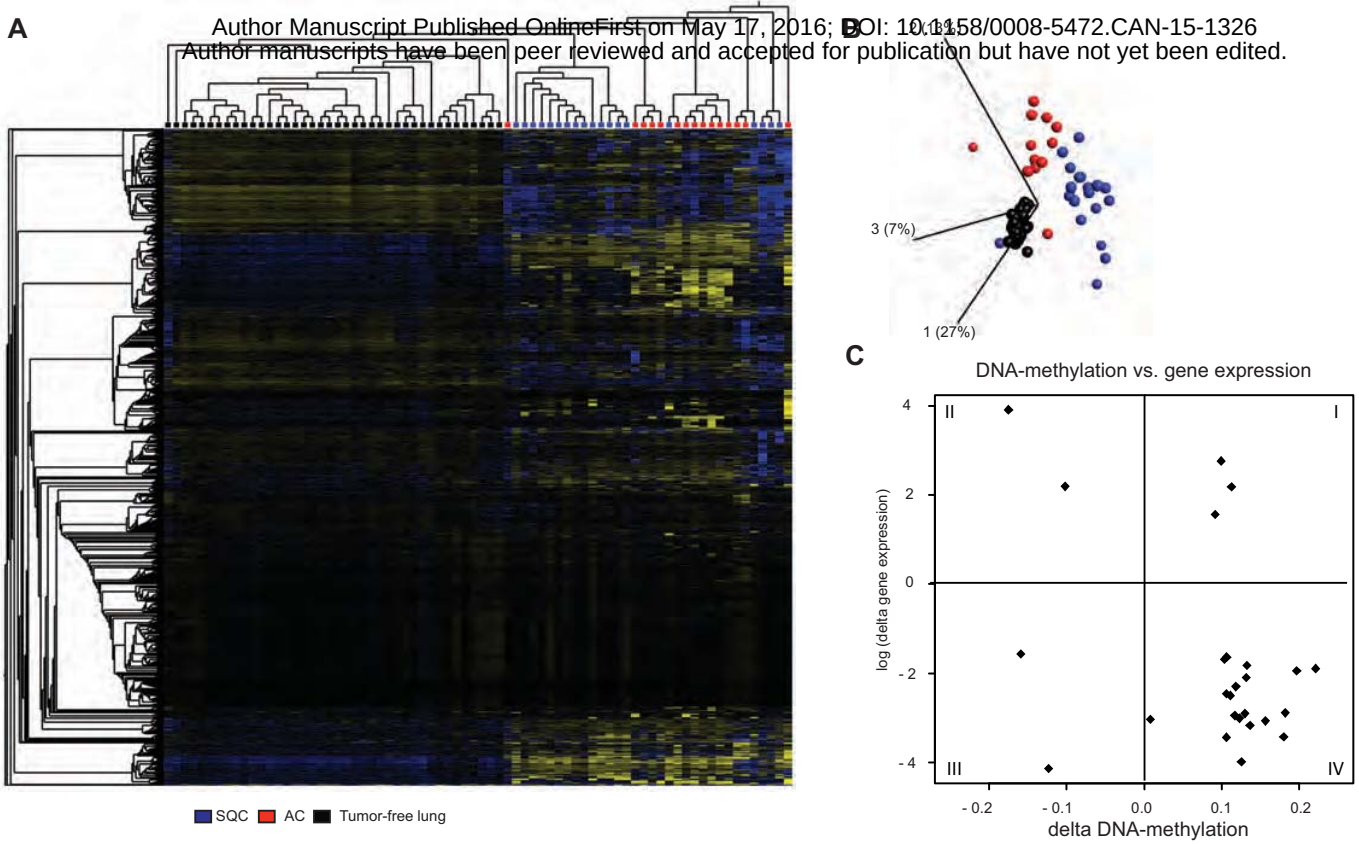

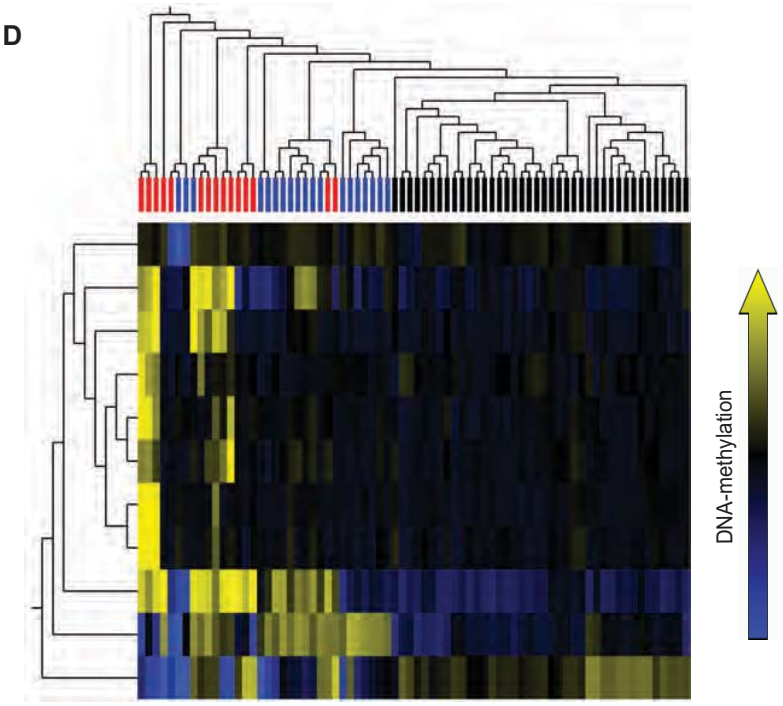

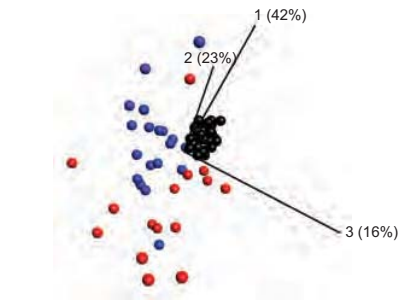

Marwitz et al., Figure 3

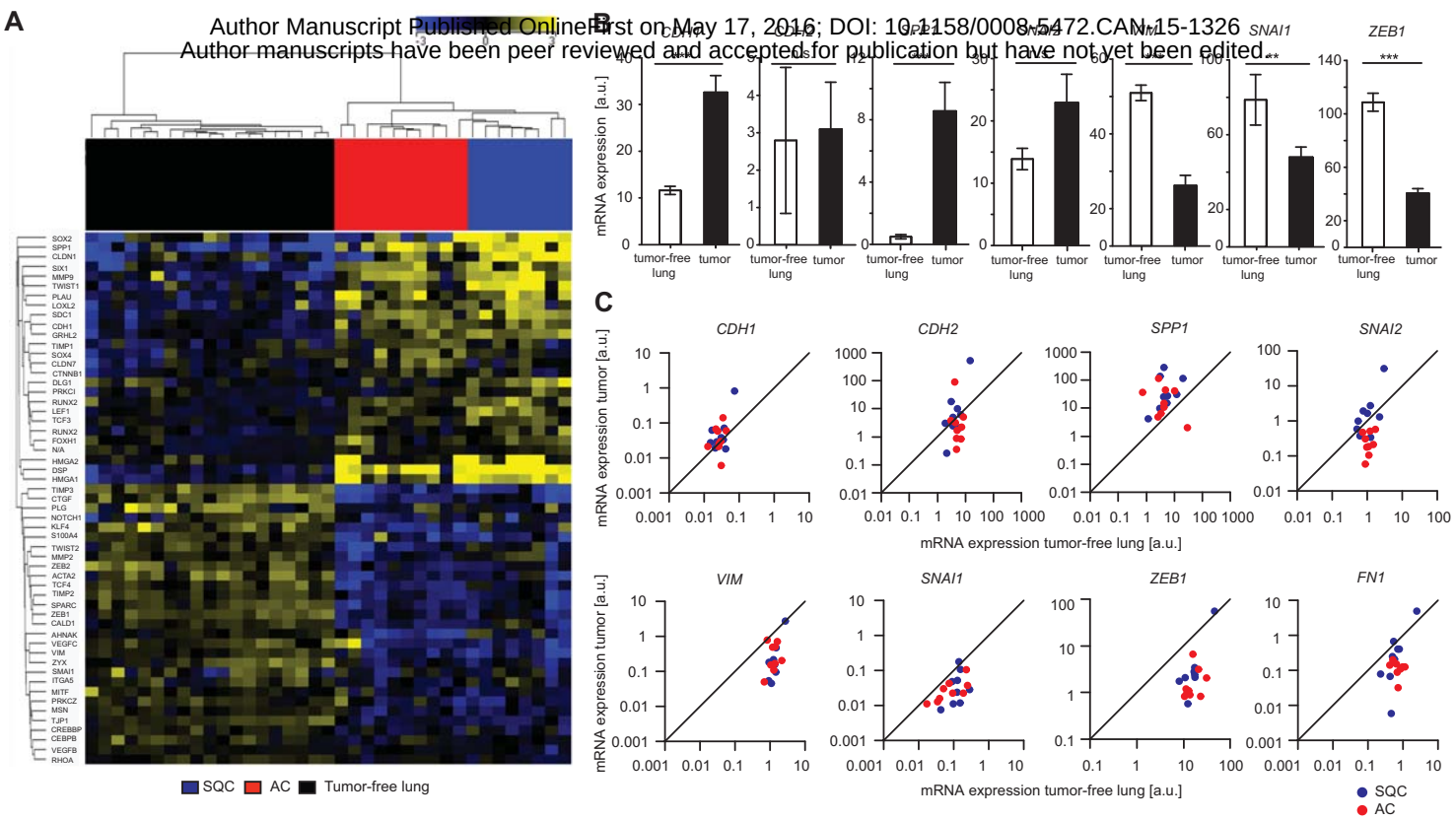

Marwitz et al., Figure 4

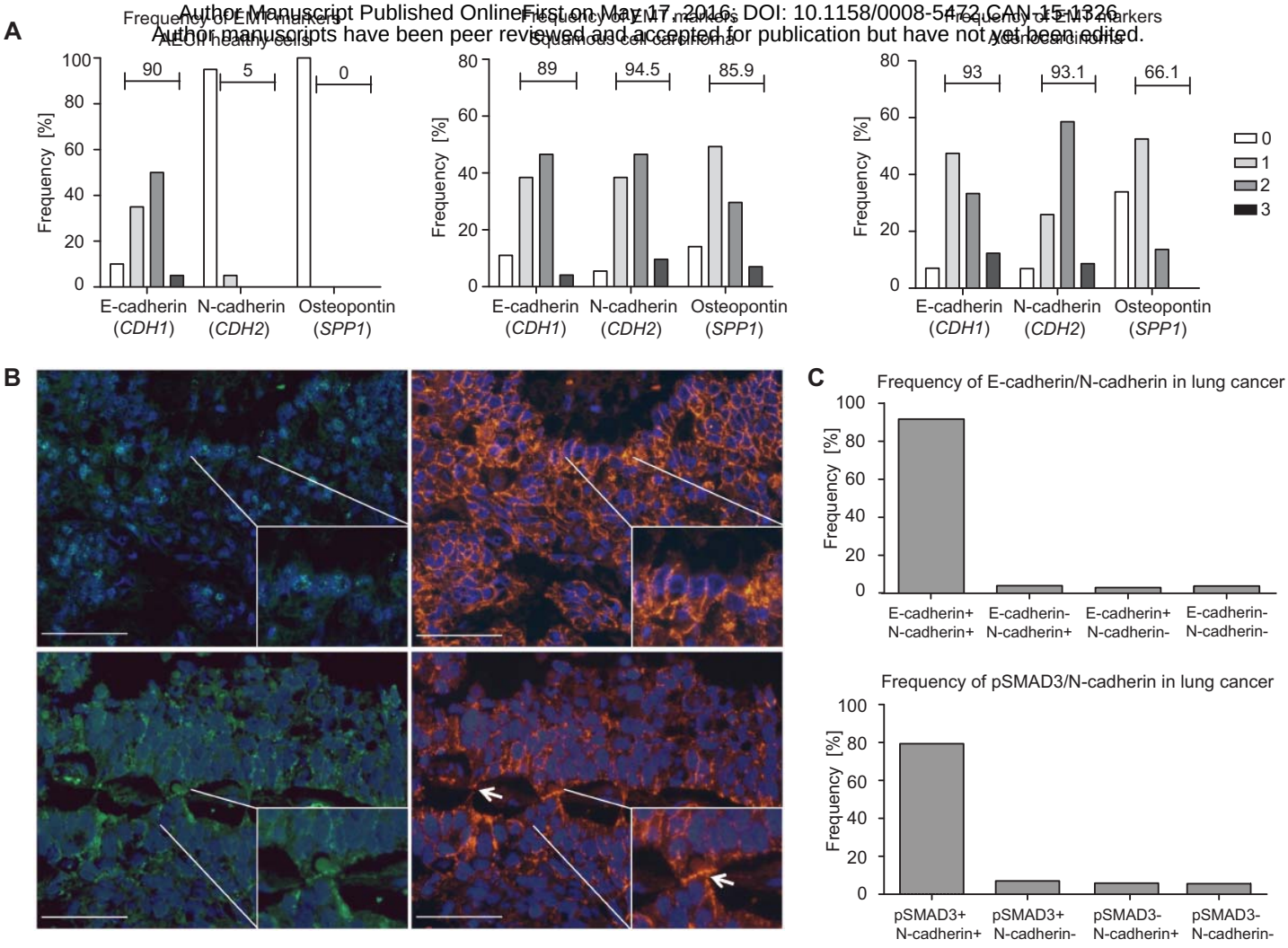

Marwitz et al., Figure 5

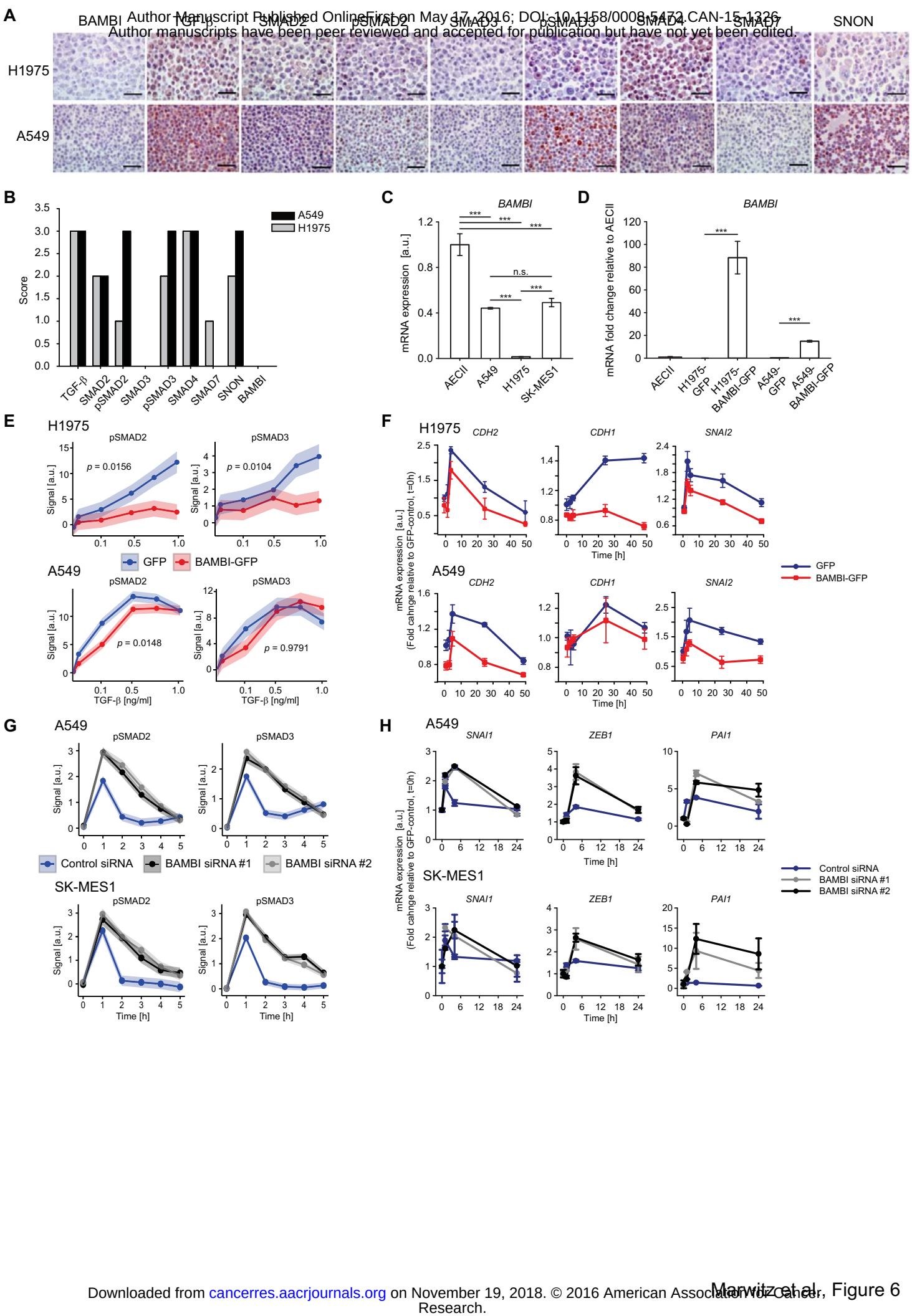

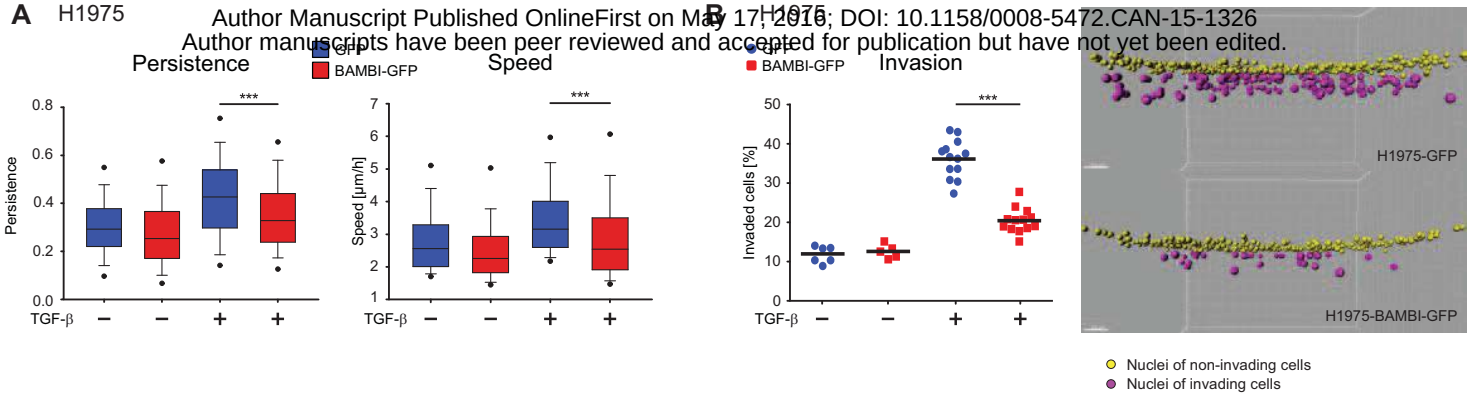

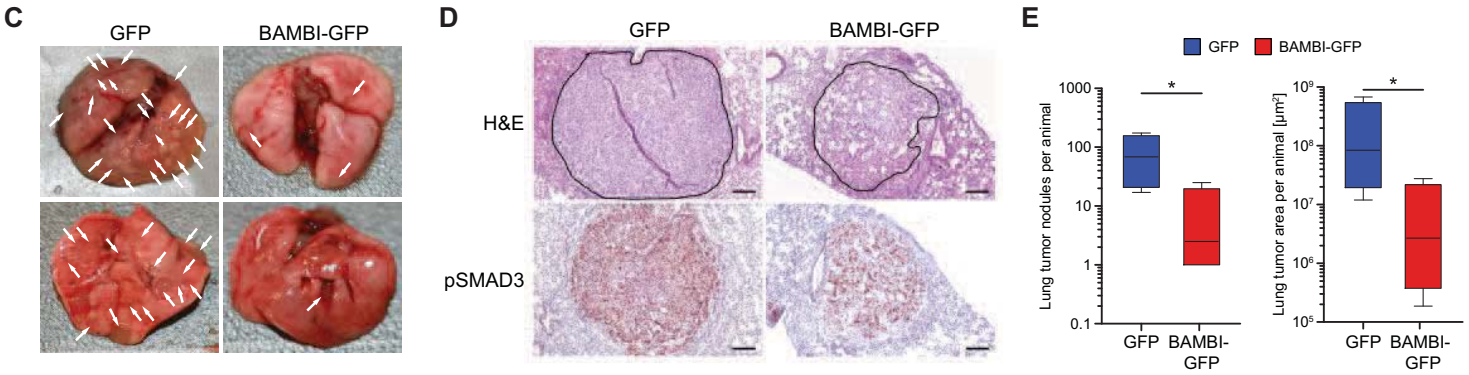

Marwitz et al., Figure 7

AACR American Association for Cancer Research

Cancer Research

The Journal of Cancer Research (1916–1930) | The American Journal of Cancer (1931–1940)

Downregulation of the TGF-β pseudoreceptor BAMBI in non-small cell lung cancer enhances TGF- β signaling and invasion

Sebastian Marwitz, Sofia Depner, Dmytro Dvornikov, et al.

Cancer Res Published OnlineFirst May 17, 2016.